Immunity

Macrophage PPARγ, a lipid activated transcription factor controls a growth factor GDF3 and skeletal muscle regeneration

--Manuscript Draft--

Manuscript Number:	IMMUNITY-D-15-00819R4
Full Title:	Macrophage PPARγ, a lipid activated transcription factor controls a growth factor GDF3 and skeletal muscle regeneration
Article Type:	Research Article
Keywords:	PPARg; GDF3; Repair macrophage; muscle regeneration; Myoblast fusion
Corresponding Author:	Laszlo Nagy Sanford Burnham Prebys Medical Discovery Institute Orlando, UNITED STATES
First Author:	Tamas Varga
Order of Authors:	Tamas Varga
	Rémi Mounier
	Andreas Patsalos
	Peter Gogolak
	Matthew Peloquin
	Attila Horvath
	Attila Pap
	Bence Daniel
	Gergely Nagy
	Eva Pintye
	Szilard Poliska
	Sylvain Cuvellier
	Sabrina Ben Larbi
	Brian E Sansbury
	Matthew Spite
	Chester W. Brown
	Bénédicte Chazaud
	Laszlo Nagy
Abstract:	Tissue regeneration requires inflammatory and reparatory activity of macrophages. Macrophages detect and eliminate the damaged tissue and subsequently promote regeneration. This dichotomy requires the switch of effector functions of macrophages coordinated with other cell types inside the injured tissue. The gene regulatory events supporting the sensory and effector functions of macrophages involved in tissue repair are not well understood. Here we show that the lipid activated transcription factor, PPARG, is required for proper skeletal muscle regeneration, acting in repair macrophages. PPARG controls the expression of the transforming growth factor-β (TGF-β) family member, GDF3, which in turn regulates the restoration of skeletal muscle integrity by promoting muscle progenitor cell fusion. This work establishes PPARG as a required metabolic sensor and transcriptional regulator of repair macrophages. Moreover, this work also establishes GDF3 as a secreted extrinsic effector protein acting on myoblasts and serving as an exclusively macrophage-derived regeneration factor in tissue repair.
Suggested Reviewers:	Peter Tontonoz

	UCLA ptontonoz@mednet.ucla.edu Expert on nuclear receptors and inflammation
	Chris Glass UCSD chglass@ucsd.edu Expert on nuclear receptors, inflammation, macrophages and epigenetics/genomics
	Ron Evans Salk Institute evans@salk.edu Expert on nuclear receptors, PPARg
	Bruce Spiegelmann Harvard Medical School bruce_spiegelman@dfci.harvard.edu Expert on PPARg
	Fabio Rossi UBC fabio@brc.ubc.ca Expert on muscle regeneration, inflammation
	Pura Munoz-Canoves ICREA pura.munoz@upf.edu Expert on muscle regeneration
Opposed Reviewers:	Rando Thomas Stanford School of Medicine rando@stanford.edu Competing research interest
	Ajay Chawla UCSF Ajay.Chawla@ucsf.edu Competing research interest in PPARg/muscle regeneration
	Amy Wagers Harvard Medical School amy.wagers@joslin.harvard.edu Competing research interest

SBP Medical Discovery Institute
SANFORD BURNHAM PREBYS at Lake Nona

Dr. Bruce Koppelman
Senior Editor
Immunity

RE: **IMMUNITY-D-15-00819R4**

October 17th, 2016

Via on-line submission

Dear Bruce,

I am submitting the revised version of our manuscript entitled

"**Macrophage PPARγ, a lipid activated transcription factor, controls the growth factor GDF3 and skeletal muscle regeneration**" containing the changes you requested for final approval.

I am looking forward to hearing from you.

Sincerely yours,

László Nagy, M.D., Ph.D.
Director, Genomic Control of Metabolism Program
Professor, Center for Metabolic Origins of Disease
Tel: 407-745-2150 Email: lnagy@sbpdiscovery.org

Response to reviewers

We have implemented the requested editorial changes.

Graphical Abstract

IMMUNITY-D-15-00819R4

Macrophage PPARγ, a lipid activated transcription factor controls a growth factor GDF3 and skeletal muscle regeneration

Tamas Varga[1,12], Rémi Mounier[2,12], Andreas Patsalos[1], Péter Gogolák[3], Matthew Peloquin[4], Attila Horvath[1], Attila Pap[1], Bence Daniel[1,4], Gergely Nagy[1,5], Eva Pintye[6], Szilárd Póliska[1], Sylvain Cuvellier[7], Sabrina Ben Larbi[2], Brian E. Sansbury[8], Matthew Spite[8], Chester W. Brown[9,10,11], Bénédicte Chazaud[2,7,*] and Laszlo Nagy[1,4,5,*]

[1] Department of Biochemistry and Molecular Biology, University of Debrecen, Debrecen, H-4012, Hungary
[2] Institut NeuroMyogène, INMG, Université Claude Bernard Lyon 1, CNRS UMR5310, Villeurbanne 69100, INSERM U1217, France
[3] Department of Immunology, University of Debrecen, Debrecen, H-4012, Hungary
[4] Sanford-Burnham-Prebys Medical Discovery Institute at Lake Nona, 6400 Sanger Road, Orlando, FL 32827
[5] MTA-DE "Lendület" Immunogenomics Research Group, University of Debrecen, Debrecen, H-4012, Hungary
[6] Department of Radiation Therapy, University of Debrecen, Debrecen, H-4012, Hungary
[7] Institut Cochin, INSERM U1016, CNRS, UMR8104, Université Paris Descartes, Sorbonne Paris Cité, Paris 75014, France
[8] Center for Experimental Therapeutics & Reperfusion Injury, Department of Anesthesiology, Perioperative and Pain Medicine, Brigham and Women's Hospital, Harvard Medical School, Boston, MA, 02115
[9] Department of Molecular and Human Genetics, Baylor College of Medicine, Houston, TX 77030
[10] Department of Pediatrics, Baylor College of Medicine, One Baylor Plaza, Houston, TX 77030
[11] Texas Children's Hospital, Houston, TX 77030

[12] Equal contribution

* Corresponding authors:
Laszlo Nagy (Lead Contact)
e-mail: lnagy@sbpdiscovery.org
phone: +1-407-745-2150
Bénédicte Chazaud
e-mail: benedicte.chazaud@inserm.fr
phone: +33-4-72431051

SUMMARY

Tissue regeneration requires inflammatory and reparatory activity of macrophages. Macrophages detect and eliminate the damaged tissue and subsequently promote regeneration. This dichotomy requires the switch of effector functions of macrophages coordinated with other cell types inside the injured tissue. The gene regulatory events supporting the sensory and effector functions of macrophages involved in tissue repair are not well understood. Here we show that the lipid activated transcription factor, PPARγ, is required for proper skeletal muscle regeneration, acting in repair macrophages. PPARγ controls the expression of the transforming growth factor-β (TGF-β) family member, GDF3, which in turn regulates the restoration of skeletal muscle integrity by promoting muscle progenitor cell fusion. This work establishes PPARγ as a required metabolic sensor and transcriptional regulator of repair macrophages. Moreover, this work also establishes GDF3 as a secreted extrinsic effector protein acting on myoblasts and serving as an exclusively macrophage-derived regeneration factor in tissue repair.

INTRODUCTION

Tissues suffer damage during an organism's lifetime. In order to maintain the body's integrity and homeostasis, it is critically important to achieve complete regeneration. In many cases a straightforward paradigm can be applied whereby organ injury induces expansion and differentiation of a quiescent population of tissue-specific stem cell-like progenitors. Impaired injury-related immune response has been shown to greatly influence regeneration in liver, central nervous system or skeletal muscle (Chazaud, 2014; Duffield et al., 2005; Laflamme and Murry, 2011; Rapalino et al., 1998). Immune cells and in particular, macrophages sense the injury, remove damaged tissues, then initiate restoration of tissue integrity *via* promoting repair mechanisms. During this latter phase the immune response regulates the reengagement of tissue progenitor cell populations to support cell growth and differentiation. Our knowledge is fragmented on how macrophages employ sensory and regulatory mechanisms and use effector functions to serve their reparatory roles. We sought to identify such integrated regulatory mechanisms that equip a macrophage with the capacity to contribute to a timely progression of repair.

We found that the fatty acid regulated transcription factor, Peroxisome Proliferator-Activated Receptor gamma (PPARγ) (Tontonoz et al., 1998), was required in repair macrophages during skeletal muscle regeneration. Mice with a deletion of PPARγ in their myeloid lineages showed a pronounced delay in regeneration. PPARγ regulated the expression of a secreted factor, GDF3 in repair macrophages. GDF3 deficiency impaired

muscle regeneration and recombinant GDF3 enhanced repair *in vivo* and the fusion of primary myogenic precursor cells (MPCs) in *in vitro* cultures. Our data reveal a PPARγ-GDF3 pathway with sensory, gene regulatory and effector components in which PPARγ in repair macrophages responds to signals and support the timely promotion of tissue repair during skeletal muscle regeneration.

RESULTS

PPARγ is expressed in macrophages of the cardiotoxin induced skeletal muscle injury model

Skeletal muscle possesses robust regenerative capacity, therefore it provides us with an excellent model system to study regeneration. The best characterized experimental model of skeletal muscle injury is the toxin induced injury and regeneration. We triggered skeletal muscle damage in the *tibialis anterior* (TA) muscle of mice by intramuscular injection of the snake venom, Cardiotoxin (CTX), to induce a homogenous and synchronous muscle damage that is repaired with the active contribution of infiltrating immune cells. We isolated macrophage populations from injured muscle and interrogated their gene expression profiles by microarray analysis. When the expression profiles of inflammatory Ly6C^{+} and repair Ly6C^{-} macrophages derived from injured muscle at day 2 CTX injury were compared, gene ontology (GO) annotation categories belonging to lipid and carbohydrate metabolism dominated the biological processes that were the most robustly upregulated in the Ly6C^{-} (repair) macrophages (Fig S1A). When analyzing the expression data, we found that a master regulator of metabolism, *Pparg*, was highly expressed in these macrophages. Using publicly available gene expression data within the Immunological Genome Project, we compared the expression of *Pparg* in muscle infiltrative macrophages to that of their direct precursors, Ly6C^{+} monocytes (Varga et al., 2013), and various other myeloid cells (Fig S1B). We found that *Pparg* in muscle macrophages was highly expressed, and that only two *in vivo* macrophage subtypes,

alveolar macrophages and splenic red pulp macrophages expressed *Pparg* higher. In contrast to *Pparg, Ppara* was not expressed in muscle infiltrative macrophages, while the expression of *Ppard* showed a declining expression in the course of regeneration (Fig S1C).

Based on these findings, we hypothesized that macrophage PPARγ is a metabolic sensor and regulator of skeletal muscle regeneration. To test this hypothesis, we used the *Pparg*$^{fl/fl}$ *Lyz2-cre* mouse strain, which is deficient in PPARγ specifically in myeloid lineages (Clausen et al., 1999). When CD45^{+} cells, which comprise all infiltrating hematopoietic cells, or sorted macrophages, were isolated from injured skeletal muscle, the expression of *Pparg* was detected in these cells by RT-qPCR (Figs S1D and S1E) in wild type (WT) animals. Furthermore, the expression of *Pparg* was greatly diminished in corresponding CD45^{+} cells and macrophages isolated from *Pparg*$^{fl/fl}$ *Lyz2-cre* animals, validating the suitability of this genetic model for these experiments.

Macrophage PPARγ regulates skeletal muscle regeneration

Wild Type and *Pparg*$^{fl/fl}$ *Lyz2-cre* animals were injected with CTX to induce TA muscle injury and then regeneration was analyzed by a combination of morphometric and flow cytometry analysis. We found *Pparg*$^{fl/fl}$ *Lyz2-cre* animals showed a pronounced delay in muscle regeneration (Figs 1A-D and S2A). First, the cross-sectional area (CSA) of the regenerating muscle fibers was significantly smaller in the *Pparg*$^{fl/fl}$ *Lyz2-cre* than in WT mice at day 8 and day 21 following CTX injury (Figs 1C and S2A). Second, there were a significantly higher number of phagocytic and/or necrotic fibers present at day 8 post

CTX in *Pparg*$^{fl/fl}$ *Lyz2-cre* mice (Figs 1A-B), indicating either a delayed clearance of dying myofibers or an altered dynamics of muscle fiber death in *Pparg*$^{fl/fl}$ *Lyz2-cre* animals. Third, increased inflammatory infiltration persisted in small regions in the regenerative areas in *Pparg*$^{fl/fl}$ *Lyz2-cre* muscles at day 8 (Fig 1A), which were resolved by day 21 (Fig S2B). Next, we wanted to ascertain whether PPARγ deficiency in the hematopoietic compartment was the major contributor to the observed phenotype. To prove this, we used a second genetic model, in which bone marrow from the epiblastic conditional ablation of *Pparg* (*Pparg*$^{fl/-}$, *Sox2-cre*$^{+}$) (Nadra et al., 2010) or WT animals were used to reconstitute the hematopoietic compartment in irradiated WT animals (bone marrow transplanted or BMT animals). TA muscles of recipient BMT animals were injected with CTX 12 weeks after BMT and histological analysis of muscle regeneration was carried out 22 days post injury. When compared with animals that received WT bone marrow (WT BMT), mice that received bone marrow deficient in PPARγ (*Pparg*$^{fl/-}$, *Sox2-cre*$^{+}$ BMT) exhibited a profound deficit in regeneration (Figs 1E-F). Further underlying the importance of PPARγ in muscle regeneration, full body *Pparg*$^{fl/-}$ *Sox2-cre*$^{+}$ animals displayed impairment in their skeletal muscle regeneration (Fig S2C).

PPARγ deficiency does not alter macrophage infiltration or differentiation in injured muscle

Several possible reasons could explain why macrophage PPARγ deficiency leads to such impairment in muscle regeneration. One underlying reason behind our observations could be a decreased macrophage infiltration in *Pparg*$^{fl/fl}$ *Lyz2-cre* animals. To monitor the

cellular dynamics of immune infiltration in CTX injured muscle, we treated WT and *Pparg*$^{fl/fl}$ *Lyz2-cre* animals with CTX, then isolated and analyzed immune cells from injured muscles on days 1, 2 or 4, using CD45^{+} magnetic bead selection. We found no major difference between the numbers and types (Ly6C^{mid} F4/80^{-} neutrophils, Ly6C^{+} F4/80^{low} and Ly6C^{-} F4/80^{high} macrophages) of infiltrating immune cells in WT *vs.* *Pparg*$^{fl/fl}$ *Lyz2-cre* animals (Fig. S3), with the exception of minor alterations in the ratio of neutrophils at day 1 and in the total number of CD45^{+} cells at day 6.

Next, we wanted to explore which macrophage functions might be relevant to muscle regeneration and regulated by PPARγ activity. To test the possible contribution of impaired phagocytosis, we used bone marrow derived macrophages (BMDMs) isolated from WT, *Pparg*$^{fl/fl}$ *Lyz2-cre* or WT BMT and *Pparg*$^{fl/-}$, *Sox2-cre*$^{+}$ BMT animals (Figs S4A-B). We set up a phagocytosis assay, in which fluorescently labeled necrotic C2C12 myoblasts were co-incubated with BMDMs labeled with a different fluorescent dye. *Pparg*$^{fl/fl}$ *Lyz2-cre* BMDMs showed no significant increase in the number of phagocyting BMDMs or in the amount of phagocytosed substrate as compared with WT BMDMs (Fig. S4B). Similar results were obtained using BMDMs derived from WT BMT or *Pparg*$^{fl/-}$, *Sox2-cre*$^{+}$ BMT animals, except that *Pparg*$^{fl/-}$, *Sox2-cre*$^{+}$ BMT BMDMs were able to phagocytose a greater load. Our results indicated that an inadequate phagocytic clearance was unlikely to be responsible for the observed delay.

Macrophage PPARγ regulates myoblast differentiation in a paracrine manner in vitro

These results led us to test if macrophage PPARγ activity confers a yet unidentified muscle differentiation-promoting phenotype to macrophages, which could explain the observed delayed muscle regeneration in animals deficient in PPARγ in macrophages. To test this hypothesis, we used *in vitro* muscle precursor cell proliferation or differentiation assays that utilize primary myoblasts isolated from WT mice (Figs 2A-B). In the first assay, we cultured primary myoblasts with conditioned medium derived from non-treated, interferon-γ (IFN-γ) or interleukin-4 (IL-4)-treated WT and *Pparg*$^{fl/fl}$ *Lyz2-cre* BMDMs, in conditions favoring cell proliferation and measured the proliferation index by detecting Ki67^{+} cells by immunofluorescence (IF). As expected, conditioned medium derived from IFN-γ-treated WT BMDMs increased myoblast proliferation (Mounier et al., 2013). Conditioned medium from non-treated *Pparg*$^{fl/fl}$ *Lyz2-cre* BMDMs phenocopied the proliferation enhancing effect of inflammatory WT BMDMs on myoblasts (Fig 2A). These results indicate that PPARγ in macrophages modulated an unknown signaling system that could influence myoblast proliferation in a paracrine manner. Next, we tested the effect of BMDM derived conditioned media on the differentiation of myoblasts by counting the number of cell nuclei within freshly formed desmin positive myotubes cultured in differentiation medium (Fig 2B and Fig S4C). As expected, we observed a large increase in differentiation when myoblasts were grown in conditioned medium derived from IL-4-treated WT BMDMs. Importantly, this increased differentiation was abrogated when conditioned medium from IL-4-treated *Pparg*$^{fl/fl}$ *Lyz2-cre* BMDMs was added to differentiating myoblasts. This effect was seen in several, independently isolated primary myoblast cell lines that were used for the experiments (Fig S4C). BMDM supernatant derived from IFN-γ-treated cells, on the

other hand, did not alter myoblast differentiation (Fig S4D). Our results raised the possibility that similar PPARγ–dependent paracrine signaling events took place *in situ* during regeneration, where muscle infiltrative macrophages and MPCs might interact to achieve a synchronized and timely regeneration.

PPARγ regulates cell type specific genes in muscle infiltrating macrophages

Next, we set out to identify PPARγ–dependent regulatory circuits that connect macrophages to myotube differentiation in a paracrine manner. As PPARγ is a transcription factor, we presumed that a relevant change in the gene expression in muscle macrophages must shed light on the regulatory circuit that is abrogated in *Pparg*$^{fl/fl}$ *Lyz2-cre* macrophages. We isolated populations of macrophages from regenerating muscle from WT and *Pparg*$^{fl/fl}$ *Lyz2-cre* animals and analyzed their gene expression profiles by microarrays (Figs 2C-E and S4E-F). We selected inflammatory Ly6C^{+} macrophages at day 1 and 2, and repair Ly6C^{-} macrophages at day 2 and 4 post CTX injury and compared their gene expression by 2 way ANOVA tests (Table S1). We created heat maps for all 4 examined macrophage subsets (Fig 2C). These heatmaps show all genes that were differentially expressed in one relevant subset and also show the expression pattern of these genes in all the other macrophage subsets. The top 5 genes that were most differentially regulated in WT *vs.* *Pparg*$^{fl/fl}$ *Lyz2-cre* cells are shown in Fig. 2D. The number of genes that were concordantly regulated in a PPARγ–mediated manner in more than one macrophage subtypes is shown in Fig. 2E. We hypothesized those genes could be under regulation by PPARγ that were expressed differently in more than one subtype

of muscle macrophages. Accordingly, we combined the lists of upregulated genes reported by the ANOVA analysis of WT *vs.* *Pparg*$^{fl/fl}$ *Lyz2-cre* comparisons. Although many genes were differentially regulated in a single type of muscle macrophages, only 5 genes (*Saa3*, *Hebp1*, *Plxnd1*, *Apold1*, *Tsg101*) were upregulated in all 4 investigated subtypes of PPARγ deficient muscle macrophages (Fig 2E and table S1). Next, we analyzed the gene sets that were downregulated in *Pparg*$^{fl/fl}$ *Lyz2-cre* macrophages. There was only 1 gene, namely Growth differentiation factor 3 (*Gdf3*), that was consistently downregulated in all 4 investigated macrophage populations (Figs 2D-E). Thus, we identified several putative PPARγ target genes that showed consistent PPARγ dependency in more than one muscle macrophage subsets. To ascertain the PPARγ–dependent regulation of some representative genes, we measured the mRNA expression of *Gdf3*, *Apold1*, *Hebp1* and *Plxnd1* by RT-qPCR in macrophage subsets sorted from injured muscle (Fig S5A). This analysis confirmed the results derived from the microarray experiments. The expression pattern of a short panel of previously described PPARγ-dependent (M2) alternative genes (Odegaard et al., 2007) indicated that the repair macrophages in CTX injured muscles were not canonical M2 macrophages, and that PPARγ exerted little, if any, influence on their expression (Fig S5B). Along the same line, while a total body deficiency in STAT6, the master regulator of IL4 signaling, caused increased presence of phagocytic and/or necrotic fibers at day 8 (Fig S5C), it did not affect the CSA of new myofibers (Fig S5D).

The genes we identified as PPARγ-dependent in muscle macrophages did not belong to the group of canonical PPARγ–regulated genes described in various myeloid cells in earlier studies (such as *Plin2*, *Cd36*, *Angptl4* or *Fabp4*) (Szanto et al., 2010; Welch et al.,

2003). One possible reason for this discrepancy could be that most *in vitro* studies apply synthetic or natural ligands of PPARγ to study the transcriptional activity of the receptor upon ligand activation. Therefore, we wanted to see if synthetic PPARγ ligand activation of infiltrating macrophages gave rise to transcriptional changes that are more reminiscent of the list of previously identified PPARγ target genes. For this reason we treated WT animals with rosiglitazone (RSG) *via* gavage and analyzed the ligand dependent gene expression changes in macrophages (Figs S4F and S5E, and Table S1). We found that many more genes were regulated by RSG treatment in Ly6C^{+} than in Ly6C^{-} cells. Again, the genes that showed differential expression upon RSG treatment in Ly6C^{+} cells did not contain established PPARγ–regulated genes, nor the 6 differently regulated genes that appeared to be under PPARγ regulation in all macrophage subsets. Although RSG treatment caused the differential regulation of fewer genes in Ly6C^{-} cells, the most robustly upregulated gene was *Angptl4*, one of the best-characterized PPARγ target genes. This suggests that not only Ly6C^{-} macrophages at day 2 expressed PPARγ, but that the receptor was also sensitive to the activating effect of an exogenous ligand in Ly6C^{-} cells. It is important to note that *Gdf3*, the gene that was found to be consistently downregulated in *Pparg*$^{fl/fl}$ *Lyz2-cre* macrophage subsets, was also regulated by RSG treatment (only) in Ly6C^{-} macrophages. Next, we took the list of 43 genes that showed ligand dependent upregulation in Ly6C^{-} macrophages upon RSG treatment and created a heat map representation to see how these genes were regulated in the absence of RSG treatment (Fig S5E). Even without RSG treatment, most of the otherwise RSG dependent genes showed a characteristic induction as Ly6C^{+} macrophages differentiated into Ly6C^{-} cells and an even further induction by day 4. This observation raised the intriguing

possibility that the underlying reason behind the limited number of PPARγ ligand regulated genes in Ly6C$^-$ macrophages was that most of these genes were already induced during muscle regeneration, even in the absence of exogenous synthetic ligand treatment. Related to this hypothesis, we detected a dynamic *in situ* regulation of eicosanoid synthesis during regeneration. While inflammatory eicosanoids (*e.g.* PGE_2 and $PGF_{2\alpha}$) were detectable in the early inflammatory stages of injury, they were later replaced by lipid mediators produced by murine 12/15-lipoxygenase (*Alox15*) that have been implicated in ligand activation of PPARγ such as 12-HETE and 15-HETE (Fig. S5F) (Huang et al., 1999).

GDF3 is a macrophage-derived PPARγ–dependent member of the TGF-ß family

To focus on putative PPARγ regulated genes whose activity could promote muscle regeneration, we interrogated the list of differently expressed genes for genes that (1) were PPARγ–dependent in more than one macrophage subset, (2) coded a secreted factor and (3) whose activity might be linked to muscle differentiation. Of note, one gene, *Gdf3* (Levine and Brivanlou, 2006; Levine et al., 2009; Shen et al., 2009), fit all these criteria. *Gdf3* was statistically significantly downregulated in *Pparg*$^{fl/fl}$ *Lyz2-cre* cells in all four investigated macrophage subsets (Figs 2 D-E, Table S1). GDF3 belongs to the TGF-β family, whose members are secreted factors acting in a paracrine manner. Finally, several members of the TGF-β family are known regulators of muscle regeneration, including GDF8 (also known as Myostatin) (McPherron et al., 1997). Therefore, we selected *Gdf3*

as the most likely PPARγ–dependent gene that contributes to muscle regeneration for further analysis.

PPARγ occupies a complex set of active enhancers around the Gdf3 locus

Next, we wanted to characterize the genomic events that are responsible for the regulation of *Gdf3* by PPARγ. We elected to use BMDMs, a readily available *in vitro* model system that allowed us to employ high-throughput genomic and epigenomic methods to interrogate the regulatory mechanism exerted by PPARγ on the *Gdf3* locus. We established that WT and *Pparg*$^{fl/fl}$*Lyz2-cre* BMDMs provided a platform with good correlation to study the PPARγ–dependent regulation of *Gdf3*, as PPARγ deficiency in BMDMs abrogated the expression of both the canonical PPARγ target gene *Angptl4* and that of *Gdf3* (Fig 3A). Then, we compiled epigenomic and genomic data to identify the relevant enhancers that were active and possibly under PPARγ regulation in BMDMs (Fig 3B). We included CTCF as a binding factor of insulator regions and RAD21, as a component of the cohesin complex to determine the boundaries of potential chromatin loops or topological domains, PU.1 as a key lineage determining factor in macrophages, RXR (the obligate heterodimeric partner of PPARγ), and PPARγ ChIP-seq data derived from thioglycolate elicited peritoneal macrophages and adipocytes. We combined these data with active epigenetic marks from H3K4me3 ChIP-seq experiments and GRO-seq data from BMDMs. Based on the common CTCF and RAD21 binding sites (Daniel et al., 2014; Merkenschlager and Odom, 2013), the transcription unit of *Gdf3* appeared to be approximately between approximately -50 kb to +50 kb. Our definition of putative, active

enhancers included: (1) binding of PU.1, (2) presence of detectable enhancer transcript (GRO-seq signal) (3) RXR or PPARγ binding. This approach was validated by applying the same criteria to the *Angptl4* locus, in which we readily identified its PPARγ–dependent enhancer (Fig S6A). Based on these criteria we nominated 14 putative active enhancers at a distance from +38 Kb to -47 Kb relative to the transcription start site of *Gdf3* (Figs 3B and S6B). As we show in Fig 3C, binding of PPARγ and RXR could be readily detected on 5 of these selected enhancers (at +7.3 kb, -21kb, -25kb, -44kb and -47kb) if we compared WT to *Pparg*$^{fl/fl}$ *Lyz2-cre* BMDMs. These data strongly suggested that *Gdf3* was regulated by one or several of these PPARγ:RXR binding sites.

GDF3 is a regulator of myoblast proliferation, differentiation and muscle regeneration

Next, we analyzed the GDF3 protein expression in whole muscle lysates of CTX injured WT mice, which provided a snapshot of GDF3 protein level during regeneration. The protein expression followed the induction seen at the mRNA level in macrophages and showed a pronounced induction, which peaked at day 4 (Fig 4A), at the time when inflammation subsides and regenerative processes start to dominate within the injured muscle. Importantly, the induction of GDF3 expression was detectable in the CD45^{+} (hematopoietic) compartment and was diminished at both mRNA and protein amount in *Pparg*$^{fl/fl}$ *Lyz2-cre* animals (Figs 4B-D). Next, we further investigated GDF3 expression in alternative models of muscle injuries. We found that, similarly to CTX injury, GDF3 protein expression was induced during glycerol mediated injury and regeneration in WT but diminished in PPARγ macrophage deficient animals (Fig 4E). Furthermore, not only

the mRNA expression of *Gdf3*, but the entire panel of genes that showed strong PPARγ dependency in the CTX model, was regulated concordantly in the two models of injury (Fig 4F). GDF3 protein expression was also induced in muscle samples exposed to exposed to crush- and freeze-injuries, which a toxin-free methods (Fig 4G). Due to recent publications that reported a high tendency for false positive detection of GDF proteins in protein detection applications (Egerman et al., 2015), it is important to note that the GDF3 protein induction during CTX injury was undetectable in muscle samples from *Gdf3*$^{-/-}$ animals (Fig 4H). To summarize, GDF3 is a macrophage-derived protein whose expression is induced in various models of muscle regeneration in a PPARγ–dependent manner.

According to our model, the regeneration delay in macrophage PPARγ deficient animals was, at least partly, attributable to a diminished macrophage derived GDF3 secretion within regenerating muscles. This model posits that GDF3 deficiency in macrophages should yield impairment in regeneration comparable to what was observed in *Pparg*$^{fl/fl}$ *Lyz2-cre* animals. Indeed, muscle regeneration after CTX injury was altered in full body *Gdf3*$^{-/-}$ animals at day 8 (Figs 5A-B). It has been reported that the full body deletion of *Gdf3* shows incomplete penetrance (Shen et al., 2009), which suggests possible compensatory mechanisms. To limit their involvement and ascertain the hematopoietic source of GDF3 during muscle regeneration, we generated BMT animals reconstituted with *Gfd3*$^{-/-}$ BM. When the GDF3 chimeric animals were challenged with CTX induced muscle injury, they exhibited impairment in regeneration at day 16 and 20 (Figs 5C-D). When compared with WT BMT animals, *Gdf3*$^{-/-}$ chimeras contained more regenerating myofibers with smaller CSA and the regenerating muscle was replete with lipid

accumulations, which are hallmarks of defective muscle regeneration (Figs 5C-D). Other cell types, such as fibro-adipogenic progenitors (FAPs) are involved in muscle regeneration (Heredia et al., 2013; Lemos et al., 2015). In line with our results from the *Gdf3*$^{-/-}$ BMT experiment (Figs 5C-D) and with the mRNA and protein expression data showing GDF3 expression in the CD45^{+} compartment (Fig 4), *Pdgfra* expressing FAP cells isolated from D2 regenerating muscle barely expressed *Gdf3* and *Lyz2* mRNA (Fig. 5E), rendering the involvement of FAPs unlikely in the macrophage derived GDF3-driven effects on muscle regeneration.

To further prove the requirement for GDF3 in muscle regeneration, we injected recombinant GDF3 into CTX injured muscles of *Pparg*$^{fl/fl}$ *Lyz2-cre* mice. We found that the exogenously added GDF3 rescued the regeneration deficit seen in these animals (Fig 6A-B). To characterize the function of GDF3 in detail, we cultured primary myoblasts with or without recombinant GDF3. We found GDF3 slightly decreased myoblast proliferation (Fig 6C, left panel). We detected an even more robust effect of GDF3 on myotube formation, as myoblast cultures showed a pronounced increase in their fusion index in the presence of GDF3 (Figs 6C, right panel, and 6D). Myotube formation depends on cell motility, terminal differentiation and cell fusion. In a specific fusion assay, we showed that GDF3 was a potent inducer of myotube formation (Fig S7A), while a differentiation assay indicated that GDF3 did not affect the terminal differentiation of myoblasts into myocytes (Fig S7B).

Next, we investigated if the SMAD2 phosphorylation pathway, which is involved in the signal transduction of several TGF-β superfamily members, is engaged during muscle regeneration. We found a detectable induction of *in situ* pSMAD2 signals in muscles at

day 4 of regeneration (Fig 7A), at the time when GDF3 expression peaked in the injured muscle. Furthermore, SMAD2 phosphorylation was significantly increased during *in vitro* treatment of primary myoblasts with GDF3 (Figs 7B-C).

In search for the molecular changes triggered in muscle progenitors in the presence of GDF3, we differentiated *in vitro* primary myoblasts with or without GDF3 and interrogated the gene expression changes by RNA-Seq. First, we compared the profile of primary myoblasts and myoblast-derived myotubes that were cultured in the presence or absence of GDF3. The expression pattern of a preselected list of genes relevant to muscle differentiation (Fig 7D) validated our experimental system. Next, we compared the expression profile of differentiating myotubes cultured with or without GDF3. The list of the differentially regulated genes (Fig 7E and Table S2) showed that a limited set of transcripts were either induced or repressed in the presence of GDF3. Several of the differentially regulated genes, including *Bex1,* (Jiang et al., 2016; Koo et al., 2007), *Sgca* (Matsumura et al., 1992) and *Camk1g,* have been implicated in muscle regeneration, muscle structure and/or Ca^{2+} homeostasis, showing that macrophage derived GDF3 could elicit biologically relevant changes during muscle regeneration.

If GDF3, a macrophage derived secreted factor can regulate *in vitro* and *in situ* muscle differentiation and regeneration, then we wanted to ask if GDF3 is the only macrophage-derived TGF-β family member that is relevant in the context of CTX induced muscle injury. Therefore, we reanalyzed the transcriptomic features of muscle infiltrative macrophages to chart the expression and dynamics of the TGF-β family signaling system (Fig 7F and Fig S7C). Three ligands (*Gdf3*, *Gdf15* and *Inhba*) showed notable gene expression dynamics in muscle infiltrative macrophages. GDF3 expression peaked in

repair macrophages and showed definitive, consistent regulation by PPARγ. The two other family members (FigS7C), *Gdf15* and *Inhba*, were also regulated during muscle regeneration, and both genes exhibited partial PPARγ dependency. The PPARγ-GDF3 regulatory axis described in this study therefore identifies a sensory-regulatory-effector mechanism, by which macrophages are regulators of the tissue progenitor compartment, namely MPCs. This axis orchestrates tissue regeneration, possibly in unison with other members of the TGF-β family, leading to synchronous regeneration.

DISCUSSION

Skeletal muscle possesses excellent regenerative capacity, therefore it was striking to see that after CTX injury full body *Pparg*$^{fl/-}$ *Sox2-cre* animals showed signs of residual inflammation and impaired regeneration. The true extent of the involvement of macrophage PPARγ in the regeneration failure in these animals is unclear for several reasons, including the uncharacterized, but presumably inflammatory state of these animals and the potential involvement of non-macrophage (*e.g.* muscle) PPARγ in regeneration. Therefore we used two distinct genetic models (BMT and conditional PPARγ deficiency, *Pparg*$^{fl/fl}$ *Lyz2-cre*), which allowed us to focus on the role of PPARγ in macrophages. The delay in regeneration in macrophage PPARγ–deficient animals was less profound than in the epiblastic *Pparg*$^{-/-}$ mice, yet it was detectable as long as three weeks after the initial injury, thus appearing to be among the most dramatic reported deficiencies in regeneration caused by impairments in macrophage functions (Mounier et al., 2013).

Our analysis did not reveal a gross difference in macrophage number or differentiation in *Pparg*$^{fl/fl}$ *Lyz2-cre* animals, unlike two other reported experimental systems where AMPK or IGF1 deficiency in muscle infiltrative macrophages led to altered macrophage differentiation (Mounier et al., 2013; Tonkin et al., 2015). Although alternatively activated macrophages have been implicated in tissue repair and PPARγ has been reported to be a regulator of alternative macrophage polarization (Odegaard et al., 2007), we have previously reported that muscle Ly6C^{+} and Ly6C^{-} macrophages do not correspond to canonical alternatively polarized macrophage populations (Varga et al.,

2016) in the CTX model. Therefore it is not surprising that, in this model PPARγ is controlling genes other than alternative macrophage related ones, reported to be PPARγ–dependent in other tissue compartments and contexts (Odegaard et al., 2007). The fact that the regeneration impairment in *Stat6*$^{-/-}$ animals did not manifest in a decrease in CSA, also suggest that PPARγ, in this experimental context, acts through mechanisms other than modulating alternative macrophage activation. Systematic transcriptomic analyses, however, provided clues about both the sensory and the regulatory roles of PPARγ in muscle infiltrating macrophages. It is important to stress that earlier descriptions of direct PPARγ transcriptional target genes often reported lipid metabolic genes as the main targets PPARγ of in macrophages, which could poorly explain the anti-inflammatory role of the receptor (Szanto et al., 2010; Welch et al., 2003). We report here that the transcriptional activity of PPARγ is unique in muscle macrophages, because the most robustly changing genes (such as *Saa3*, *Hebp1*) were linked to inflammation, rather than to lipid metabolism. Second, *in vivo* treatment with RSG identified the Ly6C^{-} repair macrophages as an *in situ* macrophage subtype that could be activated by a synthetic ligand for PPARγ. The surprising fact that RSG treatment elicited characteristically different gene expression changes in Ly6C^{+} and Ly6C^{-} macrophages isolated from the same tissue and timepoint underscores the notion that distinct macrophage subsets have differential responses to environmental cues. A possible interpretation of the available data would be the involvement of a yet unidentified endogenous ligand for PPARγ whose activity is restricted to the Ly6C^{-} compartment, which could explain the tendency of otherwise RSG inducible genes to be upregulated in the Ly6C^{-} macrophages even in the absence of the synthetic ligand.

Whether the dynamic regulation of *in situ* eicosanoid synthesis we detected during regeneration could be behind the apparent ligand activation of the receptor, requires further investigation.

From the perspective of muscle regeneration, the most notable finding was the identification of GDF3, a TGF-β family member, which showed consistent regulation by PPARγ in all relevant macrophage subtypes. To ascertain that GDF3 was not only a PPARγ dependent factor, but also a direct PPARγ target, we analyzed an extensive range of genomic and epigenomic data. Although it is clear that GDF3 is expressed in a PPARγ-dependent fashion and can be induced by ligand in muscle derived $Ly6C^-$ macrophages, direct regulation by PPARγ is challenging to prove, because ligand dependent regulation appears to be macrophage subtype specific and not detectable in BMDMs. However, we have provided data that are consistent with direct regulation, even in BMDMs.

It is noteworthy, that both GDF3 gene and protein expressions were much lower in the $CD45^-$ fraction isolated from injured muscle than in the hematopoietic compartment. Considering that the separation of $CD45^+$ cells is inherently incomplete, our results indicate that macrophages are the predominant, if not the only source of GDF3 within the injured tissue. This exclusivity sets GDF3 apart from other macrophage derived regenerative factors, such as IGF1 (Tonkin et al., 2015), which is also produced by muscle and in the liver upon injury. The timing and localization of GDF3 protein in the CTX and other, unrelated injury models firmly suggested that GDF3 is a general, macrophage specific regulator of muscle regeneration.

To link macrophage biology to tissue regeneration, we analyzed the role of macrophage derived GDF3 in muscle regeneration in a combination of *in vivo* and *in vitro* approaches. Foremost, two genetic models of GDF3 deficiency reported a delay in regeneration. While the decrease in average CSA in *Gdf3*$^{-/-}$ animals was comparable to that seen in *Pparg*$^{fl/fl}$ *Lyz2-cre* animals, *Gdf3*$^{-/-}$ animals did not display persistent inflammation and delayed resolution of necrotic and/or phagocytic fibers. This suggested that PPARγ regulated several relevant pathways during regeneration. Notably, a gain of function experiment revealed that exogenous GDF3 could counteract the deleterious effect PPARγ deficiency in macrophages. Our *in vitro* results with BMDM supernatants and myoblasts indicated the presence of a regulatory circuit between macrophages and muscle cells and showed that GDF3 appeared to be an especially robust enhancer of myoblast fusion.

As other cell types are also involved in the regeneration process (Heredia et al., 2013; Joe et al., 2010; Uezumi et al., 2010), it cannot be excluded that GDF3 is only one of the TGF-β family members that are active during regeneration and that it has effects on other cell types such as FAPs as well. It is remarkable, though, that the key elements of the myogenic cross talk between cell types can be modeled *in vitro* using macrophages and myoblasts only, arguing that these two cell types and their interactions are critical to support regeneration.

Our findings also carry potential implications for pathological circumstances in which recurrent muscle damage and asynchrony in repair due to genetic conditions leads to debilitating degenerative muscle diseases, such as Duchenne Muscular Dystrophy (DMD). It is of great importance to determine if GDF3 is also a regulator of muscle

regeneration in DMD or other types of myopathies, which are most of the time associated with the permanent presence of inflammatory cells, especially macrophages.

MATERIALS AND METHODS

For more detailed descriptions of experimental procedures, please see supplemental materials and methods.

Mice.

Pparg$^{fl/fl}$*Lyz2-cre*$^{+}$ and wild type C57BL/6J controls, *Pparg*$^{fl/-}$*Sox2-cre*$^{+}$ and littermate control *Pparg*$^{fl/+}$*Lyz2-cre*$^{-}$ animals, and *Gdf3*$^{-/-}$ and littermate C57BL/6 albino controls were used in the experiments. All experimental procedure conducted on animals were carried out in accordance with institutional regulations.

Muscle injury. Mice were anaesthetized with isoflurane and 50 µl of cardiotoxin ($12X10^{-6}$ mol/l in PBS) was injected in the *tibialis anterior* (TA) muscle. Muscles were recovered for flow cytometry analysis at day 1, 2 or 4 post-injury or for muscle histology at day 8 post-injury.

Histological analysis of muscle regeneration. Muscles were removed and snap frozen in nitrogen-chilled isopentane (–160°C). 8 µm thick cryosections were cut and stained with hematoxylin-eosin (HE). HE stained sections were analyzed for cross sectional area (CSA) or for the presence of phagocytic fibers. Day 8 post CTX slides were also IF stained for Desmin / F4/80 / DAPI.

Macrophage cell culture for conditioned medium generation. Macrophages were obtained from bone marrow (BM) precursor cells that were were cultured in DMEM medium containing 20% FBS and 30% conditioned medium of L929 cell line (enriched in CSF-1) for 7 days. Macrophages were activated with IFN-γ (50 ng/ml) or IL-4 (10 ng/ml) to obtain macrophage-conditioned medium.

Myogenic precursor cell (MPC) culture. Murine MPCs were obtained from TA muscle and cultured using standard conditions in DMEM/ F12 (Gibco Life Technologies) containing 20% FBS and 2% Ultroser G (Pall Inc). For proliferation studies, MPCs were incubated for 1 day with conditioned medium + 2.5% FBS or with 2.5% FBS medium containing GDF3 mouse recombinant protein. Cells were then incubated with anti-ki67 antibodies (15580 Abcam), which were subsequently visualized using cy3-conjugated secondary antibodies (Jackson Immunoresearch Inc). For differentiation studies, MPCs were incubated for 3 days with conditioned medium containing 2% horse serum or with 2% horse serum medium containing GDF3. Cells were then incubated with anti-desmin antibodies (32362 Abcam), in combination with a cy3-conjugated secondary antibody (Jackson Immunoresearch Inc).

Phagocytosis assay: BMDM cells and C2C12 cells were stained with CellVue or PKH67 (Sigma), respectively. Heat killed stained C2C12 were used as phagocytic substrates for stained BMDMs and fluorescent intensity was measured with a FACScalibur instrument.

Image capture and analysis for myoblast cultures. Fusion index (for myogenic cells) was calculated as the number of nuclei within myotubes divided by the total number of nuclei, nuclei number being estimated using the Image J software.

Isolation of macrophages from muscle. $CD45^+$ cells were isolated from CTX injected muscles using magnetic sorting (Miltenyi Biotec). $CD45^+$ cells then were labeled with fluorescently labeled antibodies and $Ly6C^+$ $F4/80^{low}$ macrophages, $Ly6C^-$ $F4/80^+$ macrophages and $Ly6C^{mid}$ $F4/80^-$ neutrophils were analyzed and sorted with a BD FACSAria III sorter.

RNA isolation from sorted MFs. Macrophage subsets were sorted from day 1, 2 and 4 post-injury muscles with a FACSAria III sorter and total RNA was isolated with TRIZOL reagent according to the manufacturer's recommendation.

Microarray analysis of muscle macrophages: Global expression pattern was analyzed on Affymetrix GeneChip Mouse Gene 1.0 ST arrays. The microarray data are publicly available (Data access: GSE71155).

ChIP (Chromatin immunoprecipitation): ChIP was carried out in BMDMs using antibodies against pre-immune IgG (Millipore, 12-370), (pan) RXR (sc-774 Santa Cruz Biotechnology) and PPARγ (Perseus #PP-A3409A).

Bioinformatic analysis of the active enhancers around the *Gdf3* and *Angptl4* locus: The list of published and/or publicly available datasets used for visualization in IGV2 to identify active enhancers can be found in the supplemental method section.

Western Blotting: GDF3 protein expression was measured using Western Blot analysis. Samples from CTX injected TA muscles or $CD45^+$ cells were lysed in RIPA buffer. GDF3 was targeted using rabbit monoclonal Anti-GDF3 primary antibody (ab109617, Abcam, Cambridge, MA) at 1:1,000 dilution in TBS-T supplemented with 5% BSA overnight at 4°C. Anti-GAPDH mouse monoclonal primary antibody (AM4300, Ambion, Carlsbad, CA) was used as a protein loading control at 1:10,000 – 1:20,000 dilution in TBS-T supplemented with 5% BSA overnight at 4°C.

RNA sequencing (RNA-Seq) library preparation for myoblast gene expression analysis: cDNA library for RNA-Seq was generated from 1μg total RNA using TruSeq RNA Sample Preparation Kit (Illumina, San Diego, CA, USA) according to the manufacturer's protocol.

The RNA-Seq data are publicly accessible (data access: PRJNA290560/SRR2136645).

General statistical analyses. All experiments were performed using at least three different samples. Student's t-tests and 2 way ANOVA analyses were performed and $P<0.05$ was considered significant ($P\leq0.05$=*, $P\leq0.01$=**, $P\leq0.0001$=***, $P\leq0.001$=****). Mean and SD values, or mean and SEM values are shown in graphs.

AUTHOR CONTRIBUTIONS

Conceptualization, TV, RM, BC and LN

Methodology, TV, AP, RM, PG, EP, BES, MS, BC, LN,

Software, AP, AH and GN

Validation, TV, RM, AP, BC

Formal analysis, TV, RM, AP, AH, GN

Investigation, TV, RM, AP, PG, MP, AP, BD, EP, SP, SC, SBL, BES, MS, CWB, BC and LN

Resources, RM, CWB, BC and LN

Writing – original draft, TV and LN

Writing – review and editing: TV, RM, MP, MS, BD, CWB, BC and LN

Visualization, TV, RM, AP, AH, GN

Funding Acquisition, BC and LN

Supervision, BC and LN

ACKNOWLEDGEMENTS

The authors acknowledge the technical assistance of Ms. T. Cseh and Ms. M. Porcelánné and discussions and comments on the manuscript by Dr. É. Rajnavölgyi and members of the Nagy laboratory. T.V. is a recipient of the RH/751/2015 intramural grant from the University of Debrecen, and a Bolyai Fellowship from the Hungarian Academy of Sciences. L.N. is supported by grants from the Hungarian Scientific Research Fund (OTKA K100196, K111941 and K116855) and by “NR-NET” ITN PITN-GA-2013-606806 from the EU-FP7 PEOPLE-2013 program. L.N and B.C. acknowledges funding

by CNRS/Hungarian Academy of Sciences Cooperation #26119 and Campus France, Balaton program #817297H. B.C. is supported by Agence Nationale de la Recherche Genopat In-A-Fibą, EU FP7 Endostem (241440) and Fondation pour la Recherche Médicale "Equipe FRM DEQ20140329495". M.S. acknowledges the support of National Institutes of Health grants HL106173 and GM095467.

REFERENCES

Chazaud, B. (2014). Macrophages: supportive cells for tissue repair and regeneration. Immunobiology *219*, 172-178.

Clausen, B.E., Burkhardt, C., Reith, W., Renkawitz, R., and Forster, I. (1999). Conditional gene targeting in macrophages and granulocytes using LysMcre mice. Transgenic research *8*, 265-277.

Daniel, B., Nagy, G., Hah, N., Horvath, A., Czimmerer, Z., Poliska, S., Gyuris, T., Keirsse, J., Gysemans, C., Van Ginderachter, J.A., *et al.* (2014). The active enhancer network operated by liganded RXR supports angiogenic activity in macrophages. Genes & development *28*, 1562-1577.

Duffield, J.S., Forbes, S.J., Constandinou, C.M., Clay, S., Partolina, M., Vuthoori, S., Wu, S., Lang, R., and Iredale, J.P. (2005). Selective depletion of macrophages reveals distinct, opposing roles during liver injury and repair. The Journal of clinical investigation *115*, 56-65.

Egerman, M.A., Cadena, S.M., Gilbert, J.A., Meyer, A., Nelson, H.N., Swalley, S.E., Mallozzi, C., Jacobi, C., Jennings, L.L., Clay, I., *et al.* (2015). GDF11 Increases with Age and Inhibits Skeletal Muscle Regeneration. Cell metabolism *22*, 164-174.

Heredia, J.E., Mukundan, L., Chen, F.M., Mueller, A.A., Deo, R.C., Locksley, R.M., Rando, T.A., and Chawla, A. (2013). Type 2 innate signals stimulate fibro/adipogenic progenitors to facilitate muscle regeneration. Cell *153*, 376-388.

Huang, J.T., Welch, J.S., Ricote, M., Binder, C.J., Willson, T.M., Kelly, C., Witztum, J.L., Funk, C.D., Conrad, D., and Glass, C.K. (1999). Interleukin-4-dependent production of PPAR-gamma ligands in macrophages by 12/15-lipoxygenase. Nature *400*, 378-382.

Jiang, C., Wang, J.H., Yue, F., and Kuang, S. (2016). The brain expressed x-linked gene 1 (Bex1) regulates myoblast fusion. Developmental biology *409*, 16-25.

Joe, A.W., Yi, L., Natarajan, A., Le Grand, F., So, L., Wang, J., Rudnicki, M.A., and Rossi, F.M. (2010). Muscle injury activates resident fibro/adipogenic progenitors that facilitate myogenesis. Nature cell biology *12*, 153-163.

Koo, J.H., Smiley, M.A., Lovering, R.M., and Margolis, F.L. (2007). Bex1 knock out mice show altered skeletal muscle regeneration. Biochemical and biophysical research communications *363*, 405-410.

Laflamme, M.A., and Murry, C.E. (2011). Heart regeneration. Nature *473*, 326-335.

Lemos, D.R., Babaeijandaghi, F., Low, M., Chang, C.K., Lee, S.T., Fiore, D., Zhang, R.H., Natarajan, A., Nedospasov, S.A., and Rossi, F.M. (2015). Nilotinib reduces muscle fibrosis in chronic muscle injury by promoting TNF-mediated apoptosis of fibro/adipogenic progenitors. Nature medicine *21*, 786-794.

Levine, A.J., and Brivanlou, A.H. (2006). GDF3, a BMP inhibitor, regulates cell fate in stem cells and early embryos. Development *133*, 209-216.

Levine, A.J., Levine, Z.J., and Brivanlou, A.H. (2009). GDF3 is a BMP inhibitor that can activate Nodal signaling only at very high doses. Developmental biology *325*, 43-48.

Matsumura, K., Tome, F.M., Collin, H., Azibi, K., Chaouch, M., Kaplan, J.C., Fardeau, M., and Campbell, K.P. (1992). Deficiency of the 50K dystrophin-associated glycoprotein in severe childhood autosomal recessive muscular dystrophy. Nature *359*, 320-322.

McPherron, A.C., Lawler, A.M., and Lee, S.J. (1997). Regulation of skeletal muscle mass in mice by a new TGF-beta superfamily member. Nature *387*, 83-90.
Merkenschlager, M., and Odom, D.T. (2013). CTCF and cohesin: linking gene regulatory elements with their targets. Cell *152*, 1285-1297.
Mounier, R., Theret, M., Arnold, L., Cuvellier, S., Bultot, L., Goransson, O., Sanz, N., Ferry, A., Sakamoto, K., Foretz, M., *et al.* (2013). AMPKalpha1 regulates macrophage skewing at the time of resolution of inflammation during skeletal muscle regeneration. Cell metabolism *18*, 251-264.
Nadra, K., Quignodon, L., Sardella, C., Joye, E., Mucciolo, A., Chrast, R., and Desvergne, B. (2010). PPARgamma in placental angiogenesis. Endocrinology *151*, 4969-4981.
Odegaard, J.I., Ricardo-Gonzalez, R.R., Goforth, M.H., Morel, C.R., Subramanian, V., Mukundan, L., Red Eagle, A., Vats, D., Brombacher, F., Ferrante, A.W., *et al.* (2007). Macrophage-specific PPARgamma controls alternative activation and improves insulin resistance. Nature *447*, 1116-1120.
Rapalino, O., Lazarov-Spiegler, O., Agranov, E., Velan, G.J., Yoles, E., Fraidakis, M., Solomon, A., Gepstein, R., Katz, A., Belkin, M., *et al.* (1998). Implantation of stimulated homologous macrophages results in partial recovery of paraplegic rats. Nature medicine *4*, 814-821.
Shen, J.J., Huang, L., Li, L., Jorgez, C., Matzuk, M.M., and Brown, C.W. (2009). Deficiency of growth differentiation factor 3 protects against diet-induced obesity by selectively acting on white adipose. Molecular endocrinology *23*, 113-123.
Szanto, A., Balint, B.L., Nagy, Z.S., Barta, E., Dezso, B., Pap, A., Szeles, L., Poliska, S., Oros, M., Evans, R.M., *et al.* (2010). STAT6 transcription factor is a facilitator of the nuclear receptor PPARgamma-regulated gene expression in macrophages and dendritic cells. Immunity *33*, 699-712.
Tonkin, J., Temmerman, L., Sampson, R.D., Gallego-Colon, E., Barberi, L., Bilbao, D., Schneider, M.D., Musaro, A., and Rosenthal, N. (2015). Monocyte/Macrophage-derived IGF-1 Orchestrates Murine Skeletal Muscle Regeneration and Modulates Autocrine Polarization. Molecular therapy : the journal of the American Society of Gene Therapy *23*, 1189-1200.
Tontonoz, P., Nagy, L., Alvarez, J.G., Thomazy, V.A., and Evans, R.M. (1998). PPARgamma promotes monocyte/macrophage differentiation and uptake of oxidized LDL. Cell *93*, 241-252.
Uezumi, A., Fukada, S., Yamamoto, N., Takeda, S., and Tsuchida, K. (2010). Mesenchymal progenitors distinct from satellite cells contribute to ectopic fat cell formation in skeletal muscle. Nature cell biology *12*, 143-152.
Varga, T., Mounier, R., Gogolak, P., Poliska, S., Chazaud, B., and Nagy, L. (2013). Tissue LyC6- macrophages are generated in the absence of circulating LyC6- monocytes and Nur77 in a model of muscle regeneration. Journal of immunology *191*, 5695-5701.
Varga, T., Mounier, R., Horvath, A., Cuvellier, S., Dumont, F., Poliska, S., Ardjoune, H., Juban, G., Nagy, L., and Chazaud, B. (2016). Highly Dynamic Transcriptional Signature of Distinct Macrophage Subsets during Sterile Inflammation, Resolution, and Tissue Repair. Journal of immunology *196*, 4771-4782.
Welch, J.S., Ricote, M., Akiyama, T.E., Gonzalez, F.J., and Glass, C.K. (2003). PPARgamma and PPARdelta negatively regulate specific subsets of lipopolysaccharide

and IFN-gamma target genes in macrophages. Proceedings of the National Academy of Sciences of the United States of America *100*, 6712-6717.

FIGURE LEGENDS

Fig 1. Impaired regeneration of skeletal muscle in PPARγ deficient animals. (A) Representative images of HE stained skeletal muscle from WT and *Pparg*$^{fl/fl}$ *Lyz2-cre* animals prior (day 0) or post CTX induced injury (day 8) are shown. Asterisk labels phagocytic and/or necrotic fibers and arrow points to foci of inflammatory infiltrations. IHC detection of desmin (red), F4/80 (green) and nuclei (blue) at day 8 post CTX injury is also shown. Scale bars in the upper left represent 50 μm. (B) The ratio of phagocytic and/or necrotic fibers relative to all regenerative fibers at day 8 of regeneration in WT and *Pparg*$^{fl/fl}$ *Lyz2-cre* muscle sections is shown. (C) Fiber size repartition of regenerating muscle in WT or *Pparg*$^{fl/fl}$ *Lyz2-cre* animals at day 8 and day 21 post CTX injury. (D) Average fiber cross section area (CSA) of regenerating muscle at indicated timepoints post CTX injury in WT and *Pparg*$^{fl/fl}$ *Lyz2-cre* animals. (E) Representative images of HE stained skeletal muscle 22 days after CTX injury from bone marrow transplanted (BMT) animals that received either WT or *Pparg*$^{fl/-}$ *Sox2-cre* bone marrow. n=4 or 4, 5 or 6, 5 or 5 and 5 or 5 muscles for WT or *Pparg*$^{fl/fl}$ *Lyz2-cre* mice, respectively, at day 0, 8, 21 and 63. (F) Muscle fiber CSA of BMT animals 22 days post CTX injury. n= 8 muscles for both genotypes. In all bar graphs, mean values +/- SEM are shown. For *Pparg* expression in macrophages and CD45^{+} cells and for additional histological analysis, see Fig S1 and S2. For the FACS analyses of infiltrating cells see Fig S3.

Fig 2. PPARγ regulated macrophage functions and genes. (A) Effect of BMDM derived conditioned media on the proliferation of primary myoblasts (+/- SEM). n= 4 or 3 for WT or *Pparg*$^{fl/fl}$ *Lyz2-cre* BMDM supernatant. (B) Effect of BMDM derived conditioned media on the differentiation of primary myotubes (+/- SEM). For the complete analysis, see Figs S4C-D. n=6 for both genotypes. (C-E) Transcriptional analysis of the Ly6C^{+} and Ly6C^{-} macrophage populations derived from WT and *Pparg*$^{fl/fl}$ *Lyz2-cre* animals. For schematics of comparisons, see Fig S4F. (C) Heatmap representation of genes that show differential (p=0.05, min. 1.5X FC) expression in the four sorted WT *vs. Pparg*$^{fl/fl}$ *Lyz2-cre* macrophages in day 1 Ly6C^{+}, D2 Ly6C^{+} and D2 Ly6C^{-}, and D4 Ly6C^{-} cells (labeled as D1 Ly6C^{+} etc.). In each heatmap, the differentially expressed genes are highlighted within a red square and the expression pattern of these genes in the other macrophage subtypes is also shown for reference. Blue and red arrows label genes that are downregulated or upregulated in WT *vs. Pparg*$^{fl/fl}$ *Lyz2-cre* cells, respectively. The blue and red arrows point to the direction of increasing fold change difference. For RT-qPCR validation of mRNA expression, see Fig S5. (D) Top 5 up and downregulated genes in the four sorted macrophage populations in *Pparg*$^{fl/fl}$ *Lyz2-cre* macrophages. Table lists gene symbols and fold change differences (FC). *Gdf3* and *Apold1*, the genes that are down-, or upregulated in *Pparg*$^{fl/fl}$ *Lyz2-cre* in all four subtypes, are highlighted in color. (E) Venn-diagrams show the overlap of the number of genes that are down-, or upregulated in *Pparg*$^{fl/fl}$ *Lyz2-cre* macrophages in the four analyzed populations.

Fig 3. *Gdf3* is a PPARγ target gene in BMDMs. (A) mRNA expression of *Angptl4*, a canonical PPARγ target gene, *Pparg*, *Gdf3* and *Apobec1*, a nearby, not regulated gene, are shown in BMDMs (n=4 for WT and n=5 for *Pparg*$^{fl/fl}$ *Lyz2-cre*). (B) Identification of possible enhancers around the *Gdf3* locus. The selection criteria for enhancers possibly involved in *Gdf3* regulation are described in the text and in Figs S6A-B. Putative enhancers are labeled by vertical lines. Blue verticals highlight enhancers without PPARγ ChIP enrichment, red verticals label enhancers where enrichment in PPARγ binding in WT BMDMs was detected by PPARγ ChIP. (C) ChIP on the putative enhancer regions reveal PPARγ binding at +7.3 Kb, -21 Kb, -25 Kb, -44 Kb and -47 Kb enhancers around the *Gdf3* locus. Representative graphs showing PPARγ, RXR or IgG ChIPs carried out on 2 samples are shown. *Angptl4* enhancer and *Gdf3* +16 kB enhancer are shown as positive and negative controls, respectively.

Fig. 4. GDF3 mRNA and protein expression in regenerating muscles. ES and B stand for embryonic stem cells and blank, respectively. (A) GDF3 protein expression in whole muscle lysates of regenerating muscles from WT mice at different timepoints (D=day). (B) GDF3 mRNA expression in CD45^{+} and CD45^{-} cells isolated at day 4 post CTX injury from WT and *Pparg*$^{fl/fl}$ *Lyz2-cre* mice (M=mouse). (C) Decreased protein expression of GDF3 in CD45^{+} cells isolated from *Pparg*$^{fl/fl}$ *Lyz2-cre* animals. (D) mRNA expression of *Gdf3* in CD45^{+} and CD45^{-} cells isolated from injured muscles at days 1, 2 and 4 post CTX in WT and *Pparg*$^{fl/fl}$ *Lyz2-cre* animals. n=4 for each day, cell type and genotype. (E) GDF3 protein expression detected in muscles lysates generated from glycerol mediated injuries (M=mouse). (F) Concordant mRNA expression pattern of PPARγ-dependent

genes in CTX and Glycerol mediated injuries. n=3 for both treatments. (G) GDF3 protein expression detected in muscle lysates generated from crush or freeze injuries (R and L stand for right and left leg, respectively). (H) Specificity of the anti-GDF3 antibody is demonstrated in day 4 CTX injured WT and *Gdf3*$^{-/-}$ muscle samples.

Fig 5. GDF3 deficiency impairs muscle regeneration. (A, B) Myofiber CSA repartition (A) and mean CSA (B) in CTX injured WT or *Gdf3*$^{-/-}$ muscles at day 8. N=7 or 7 muscles for WT or *Gdf3*$^{-/-}$ mice. (C) Representative HE stained muscle sections of WT BMT and *Gdf3*$^{-/-}$ BMT animals, 16 days post CTX injury. Scale bars represent 50 μm. n= 4 muscles for both timepoints and genotypes. (D) Myofiber CSA measurement in WT BMT and *Gdf3*$^{-/-}$ KO BMT animals, 16 and 20 days post CTX injury. (E) Lack of *Gdf3* and *Lyz2* mRNA expression in PDGFRA^{+} FAPs isolated from regenerating muscle at day 2 post-injury n=3.

Fig 6. Effects of recombinant GDF3 on muscle differentiation. (A, B) Improvement in regeneration by administration of recombinant GDF3 in *Pparg*$^{fl/fl}$ *Lyz2-cre* animals. (A) HE stained images and (B) CSA measurements are shown. (C) In vitro proliferation and differentiation assays on primary myoblasts in the presence of recombinant GDF3. n=4. (D) IF against Desmin (red) and DAPI (blue) shows a drastic enhancement of myotube formation in the presence of recombinant (r) GDF3 in the *in vitro* primary myoblast myogenesis assay n=3. In all bar graphs, bars represent mean +/- SEM. For the effect of rGDF3 on myogenic differentiation and fusion, see Fig S7. Scale bars represent 50 μm in each image in Fig. 6A and D.

Fig 7. Effects of GDF3 on myogenesis. (A) Increased pSmad2 phosphorylation in regenerating muscles peaking at day 4 post CTX injury. (B-C) Increased Smad2 phosphorylation in primary myoblasts treated with rGDF3. IF images and % of pSMAD2 positive cells are shown. n=3. (D) Heatmap representation of the expression changes of myogenic genes validating the utilized *in vitro* primary myoblast assay. (E) Heatmap representation of genes that are differentially expressed (min. fold change difference of 1.2X between differentiated myoblasts +/- rGDF3) in the presence of recombinant GDF3 during myoblast differentiation. (F) Heatmap representation of members of the TGF-β superfamily signaling system that are expressed and regulated, or expressed but not regulated in muscle derived macrophages. For non-expressed members, see Fig S7C.

Figure 1

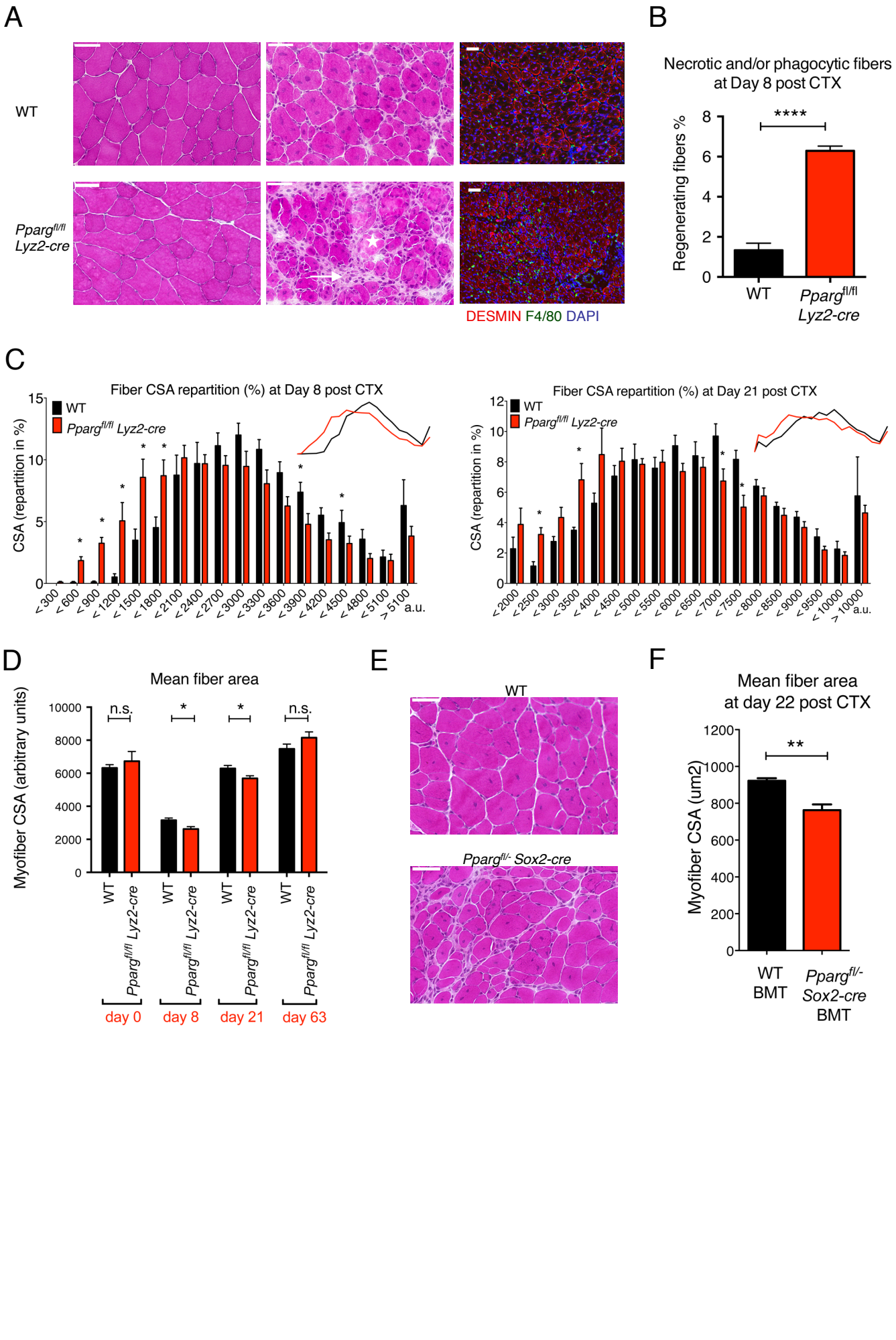
A
WT
Pparg fl/fl Lyz2-cre
DESMIN F4/80 DAPI
B
Necrotic and/or phagocytic fibers at Day 8 post CTX
Regenerating fibers %
****
WT
Pparg fl/fl Lyz2-cre
C
Fiber CSA repartition (%) at Day 8 post CTX
WT
Pparg fl/fl Lyz2-cre
CSA (repartition in %)
a.u.
Fiber CSA repartition (%) at Day 21 post CTX
D
Mean fiber area
Myofiber CSA (arbitrary units)
n.s.
day 0
day 8
day 21
day 63
E
WT
Pparg fl/- Sox2-cre
F
Mean fiber area at day 22 post CTX
Myofiber CSA (um2)
**
WT BMT
Pparg fl/- Sox2-cre BMT

Figure 2

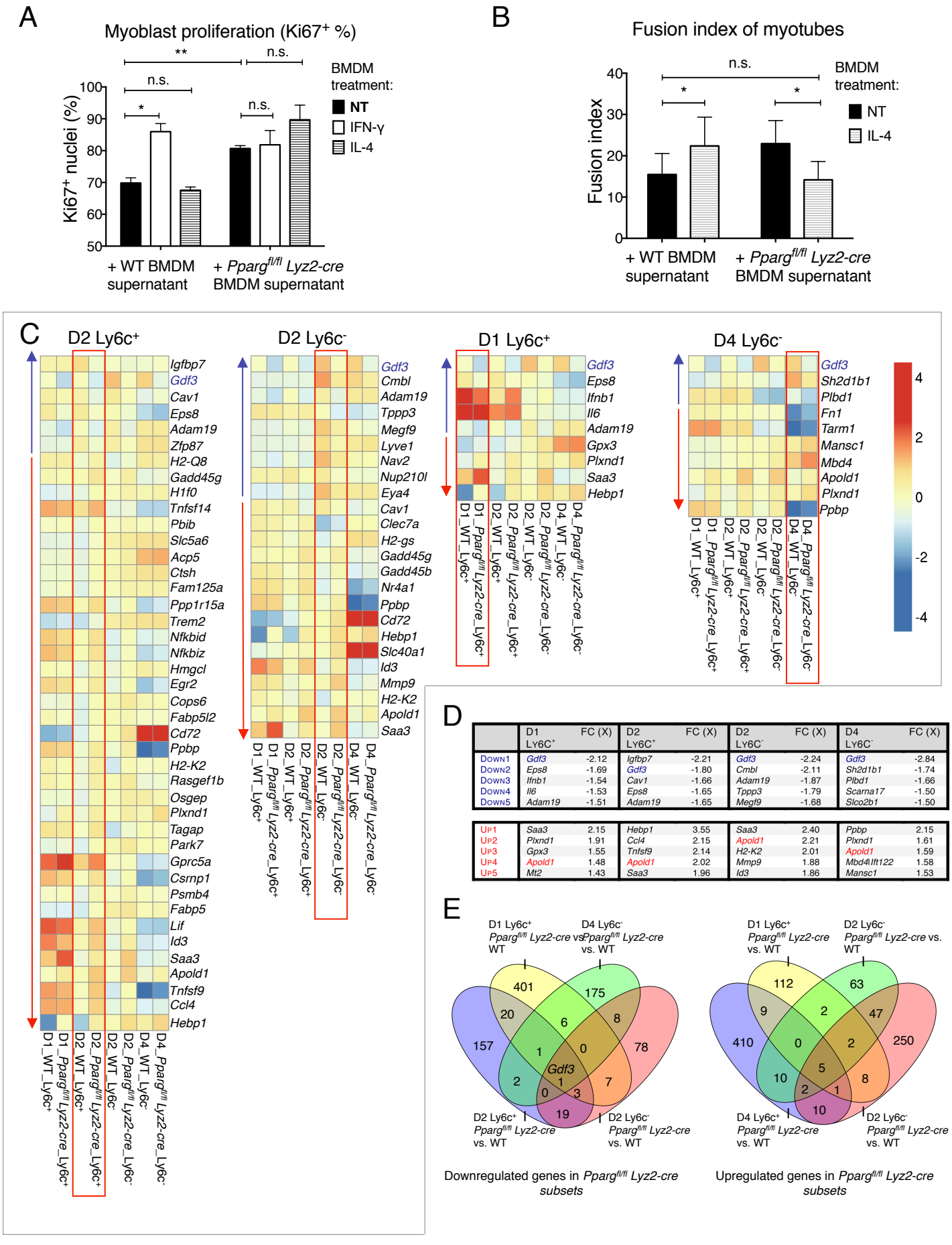

	D1 Ly6C+	FC (X)	D2 Ly6C+	FC (X)	D2 Ly6C-	FC (X)	D4 Ly6C-	FC (X)
Down1	Gdf3	-2.12	Igfbp7	-2.21	Gdf3	-2.24	Gdf3	-2.84
Down2	Eps8	-1.69	Gdf3	-1.80	Cmbl	-2.11	Sh2d1b1	-1.74
Down3	Ifnb1	-1.54	Cav1	-1.66	Adam19	-1.87	Plbd1	-1.66
Down4	Il6	-1.53	Eps8	-1.65	Tppp3	-1.79	Scarna17	-1.50
Down5	Adam19	-1.51	Adam19	-1.65	Megf9	-1.68	Slco2b1	-1.50
Up1	Saa3	2.15	Hebp1	3.55	Saa3	2.40	Ppbp	2.15
Up2	Plxnd1	1.91	Ccl4	2.15	Apold1	2.21	Plxnd1	1.61
Up3	Gpx3	1.55	Tnfsf9	2.14	H2-K2	2.01	Apold1	1.59
Up4	Apold1	1.48	Apold1	2.02	Mmp9	1.88	Mbd4Ilft122	1.58
Up5	Mt2	1.43	Saa3	1.96	Id3	1.86	Mansc1	1.53

Figure 3

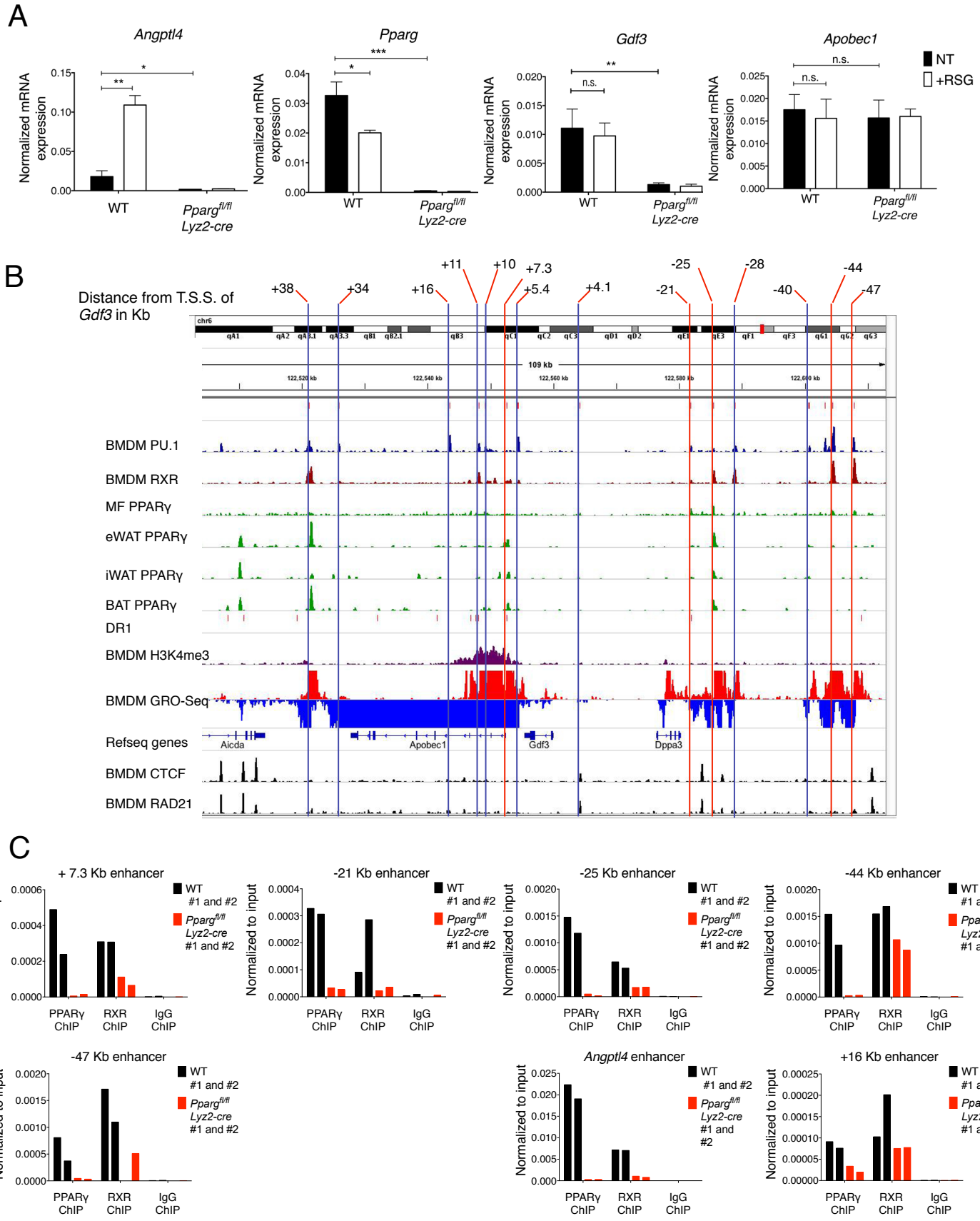
A
Angptl4
Pparg
Gdf3
Apobec1
Normalized mRNA expression
NT
+RSG
WT
Pparg fl/fl Lyz2-cre
n.s.
B
Distance from T.S.S. of Gdf3 in Kb
+38
+34
+16
+11
+10
+7.3
+5.4
+4.1
-25
-21
-28
-40
-44
-47
BMDM PU.1
BMDM RXR
MF PPARγ
eWAT PPARγ
iWAT PPARγ
BAT PPARγ
DR1
BMDM H3K4me3
BMDM GRO-Seq
Refseq genes
Aicda
Apobec1
Gdf3
Dppa3
BMDM CTCF
BMDM RAD21
C
+ 7.3 Kb enhancer
-21 Kb enhancer
-25 Kb enhancer
-44 Kb enhancer
-47 Kb enhancer
Angptl4 enhancer
+16 Kb enhancer
Normalized to input
WT #1 and #2
Pparg fl/fl Lyz2-cre #1 and #2
PPARγ ChIP
RXR ChIP
IgG ChIP

Figure 4

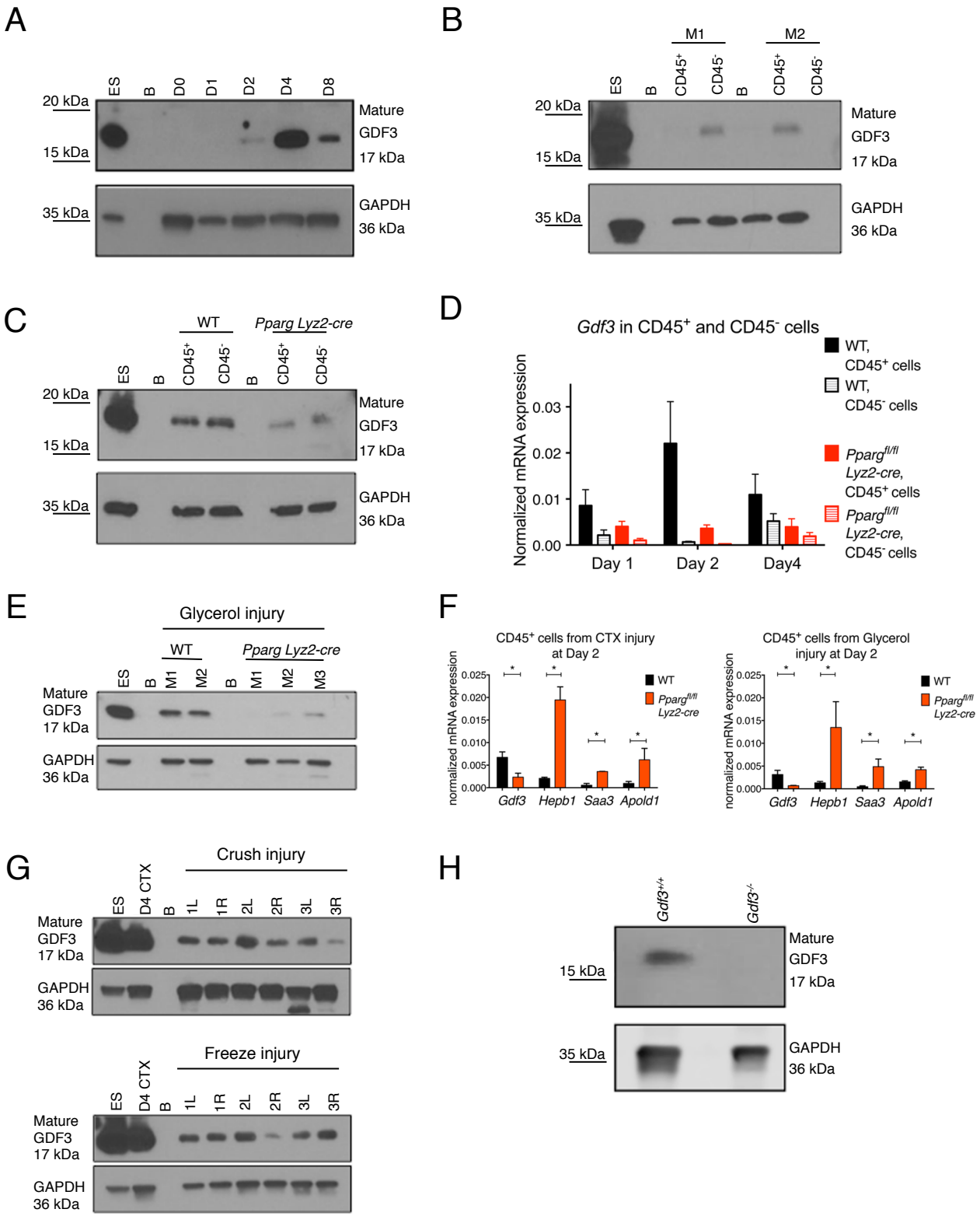
A
ES
B
D0
D1
D2
D4
D8
20 kDa
15 kDa
35 kDa
Mature GDF3 17 kDa
GAPDH 36 kDa
B
M1
M2
CD45+
CD45-
C
WT
Pparg Lyz2-cre
D
Gdf3 in CD45+ and CD45- cells
Normalized mRNA expression
WT, CD45+ cells
WT, CD45- cells
Pparg fl/fl Lyz2-cre, CD45+ cells
Pparg fl/fl Lyz2-cre, CD45- cells
Day 1
Day 2
Day4
E
Glycerol injury
M3
F
CD45+ cells from CTX injury at Day 2
CD45+ cells from Glycerol injury at Day 2
Gdf3
Hepb1
Saa3
Apold1
G
Crush injury
D4 CTX
1L
1R
2L
2R
3L
3R
Freeze injury
H
Gdf3+/+
Gdf3-/-

Figure 5

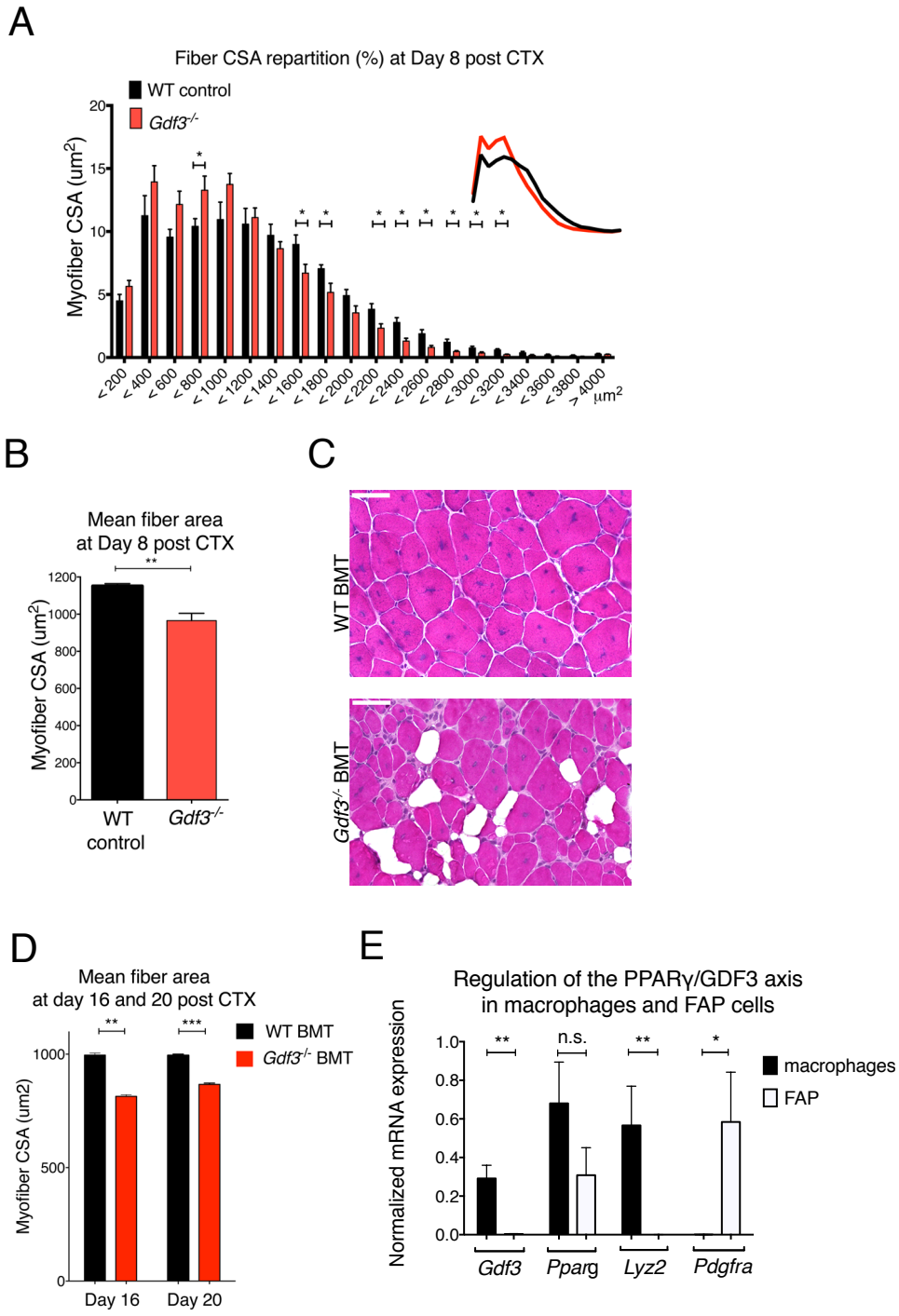
A
Fiber CSA repartition (%) at Day 8 post CTX
WT control
Gdf3-/-
Myofiber CSA (um2)
<200
<400
<600
<800
<1000
<1200
<1400
<1600
<1800
<2000
<2200
<2400
<2600
<2800
<3000
<3200
<3400
<3600
<3800
>4000
µm2
B
Mean fiber area
at Day 8 post CTX
Myofiber CSA (um2)
WT control
Gdf3-/-
C
WT BMT
Gdf3-/- BMT
D
Mean fiber area
at day 16 and 20 post CTX
WT BMT
Gdf3-/- BMT
Myofiber CSA (um2)
Day 16
Day 20
E
Regulation of the PPARγ/GDF3 axis
in macrophages and FAP cells
Normalized mRNA expression
n.s.
macrophages
FAP
Gdf3
Pparg
Lyz2
Pdgfra

Figure 6

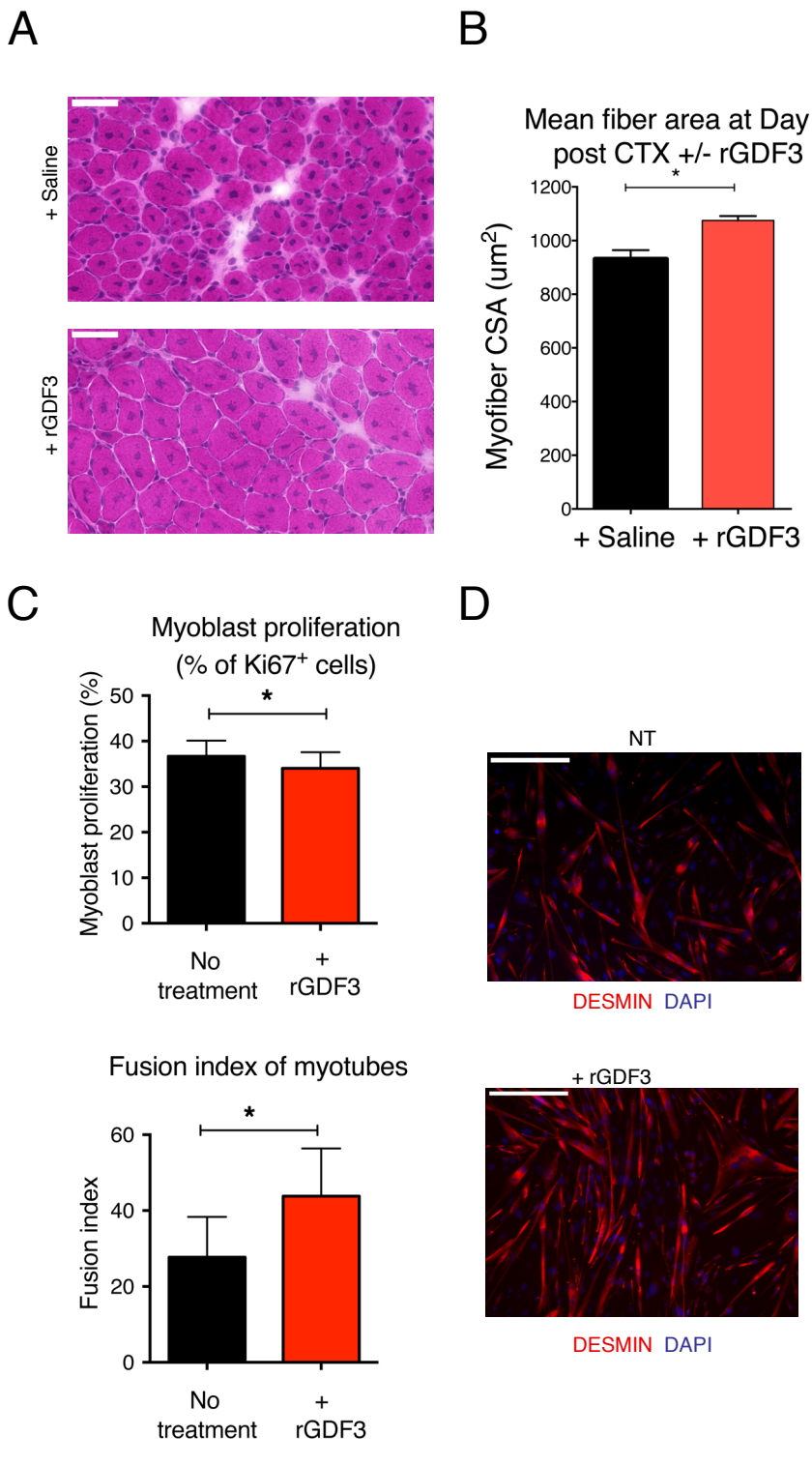
A
+ Saline
+ rGDF3
B
Mean fiber area at Day 8
post CTX +/- rGDF3
Myofiber CSA (um2)
1200
1000
800
600
400
200
0
*
+ Saline
+ rGDF3
C
Myoblast proliferation
(% of Ki67+ cells)
Myoblast proliferation (%)
50
40
30
20
10
0
*
No
treatment
+
rGDF3
Fusion index of myotubes
Fusion index
60
40
20
0
*
No
treatment
+
rGDF3
D
NT
DESMIN DAPI
+ rGDF3
DESMIN DAPI

Figure 7

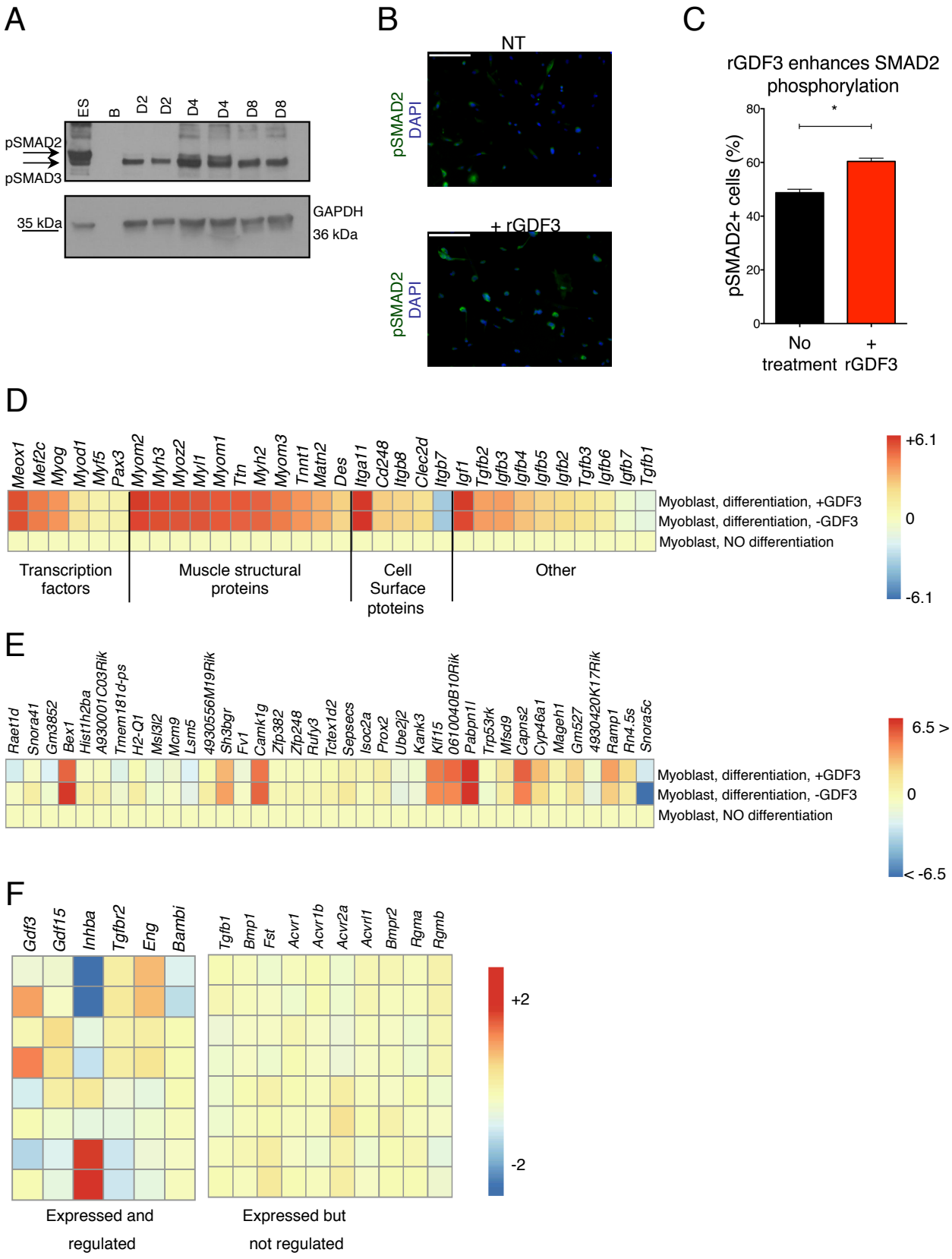
A
ES
B
D2
D2
D4
D4
D8
D8
pSMAD2
pSMAD3
35 kDa
GAPDH
36 kDa
B
NT
pSMAD2
DAPI
+ rGDF3
pSMAD2
DAPI
C
rGDF3 enhances SMAD2 phosphorylation
pSMAD2+ cells (%)
80
60
40
20
0
*
No treatment
+ rGDF3
D
Meox1 Mef2c Myog Myod1 Myf5 Pax3 Myom2 Myh3 Myoz2 Myl1 Myom1 Ttn Myh2 Myom3 Tnnt1 Matn2 Des Itga11 Cd248 Itgb8 Clec2d Itgb7 Igf1 Tgfb2 Igfb3 Igfb4 Igfb5 Igfb2 Tgfb3 Igfb6 Igfb7 Tgfb1
Myoblast, differentiation, +GDF3
Myoblast, differentiation, -GDF3
Myoblast, NO differentiation
Transcription factors
Muscle structural proteins
Cell Surface ptoteins
Other
+6.1
0
-6.1
E
Raet1d Snora41 Gm3852 Bex1 Hist1h2ba A930001C03Rik Tmem181d-ps H2-Q1 Msl3l2 Mcm9 Lsm5 4930556M19Rik Sh3bgr Fv1 Camk1g Zfp382 Zfp248 Rufy3 Tctex1d2 Sepsecs Isoc2a Prox2 Ube2j2 Kank3 Klf15 0610040B10Rik Pabpn1l Trp53rk Mfsd9 Capns2 Cyp46a1 Mageh1 Gm527 4930420K17Rik Ramp1 Rn4.5s Snora5c
Myoblast, differentiation, +GDF3
Myoblast, differentiation, -GDF3
Myoblast, NO differentiation
6.5 >
0
< -6.5
F
Gdf3 Gdf15 Inhba Tgfbr2 Eng Bambi
Tgfb1 Bmp1 Fst Acvr1 Acvr1b Acvr2a Acvrl1 Bmpr2 Rgma Rgmb
+2
-2
Expressed and regulated
Expressed but not regulated

Varga et al. Macrophage PPARγ, a lipid activated transcription factor, controls the growth factor GDF3 and skeletal muscle regeneration

SUPPLEMENTAL MATERIAL

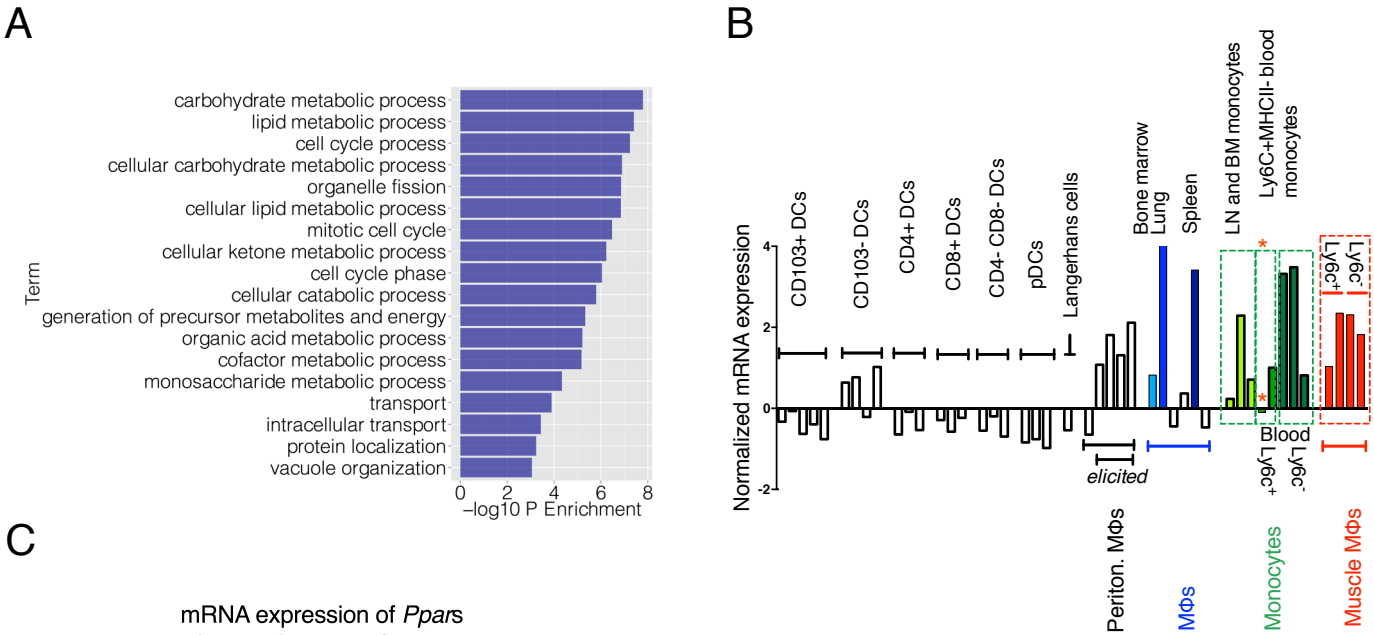

VARGA et al. Suppl Fig 1.

SUPPLEMENTAL FIGURES

Fig S1. related to Figures 1 and 2. PPARG in muscle infiltrative macrophages during skeletal muscle regeneration (A) GO analysis of the genes that are upregulated as inflammatory Ly6c^{+} macrophages differentiate into regenerative Ly6c^{-} macrophages during muscle regeneration at day 2 past CTX injury. (B) Expression of *Pparg* in various macrophages and dendritic cells. Microarray data derived from muscle derived macrophages isolated for this study and various myeloid cell populations isolated within the Immunological Genome Project were pooled and normalized together (per gene normalization to the median expression level of *Pparg*). A selected set of samples and their normalized expression value are shown. The commonly used macrophage model, bone marrow derived macrophages, are highlighted in light blue, while the high *Pparg* expressing lung macrophage and splenic red pulp macrophage are highlighted in medium and dark blue. The most likely precursor for muscle derived macrophages, Ly6c^{+} monocytes, is labeled with a red asterisk. The detailed description of all cell types is available upon request. (C) Expression of the other *Ppar* isoforms do not suggest the involvement of PPARδ or PPARα (D) Expression of *Pparg* mRNA in day 1 WT and day 2 WT or *Pparg*$^{fl/fl}$ *Lyz2-cre* CD45^{+} cells and in (E) day 2 sorted Ly6c^{+} and Ly6c^{-} MΦs isolated from CTX injured muscle. n=3 for day 1 WT CD45^{+} and n=5 or 4 for day 2 WT or *Pparg*$^{fl/fl}$ *Lyz2-cre* CD45^{+} cells. n=5 and 5 for day 2 Ly6c^{+} or Ly6c^{-} macrophages.

A

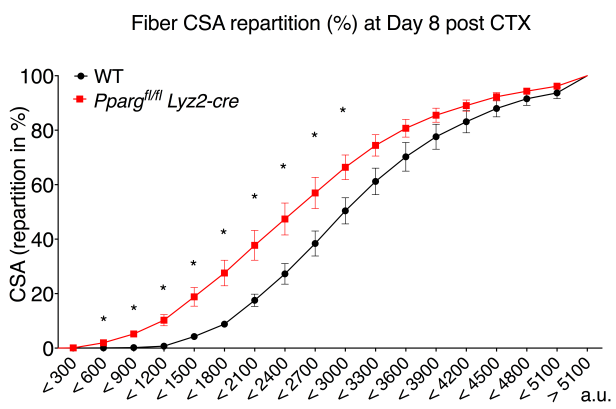
Fiber CSA repartition (%) at Day 8 post CTX
WT
Pparg fl/fl Lyz2-cre
CSA (repartition in %)
100
80
60
40
20
0
<300
<600
<900
<1200
<1500
<1800
<2100
<2400
<2700
<3000
<3300
<3600
<3900
<4200
<4500
<4800
<5100
>5100
a.u.

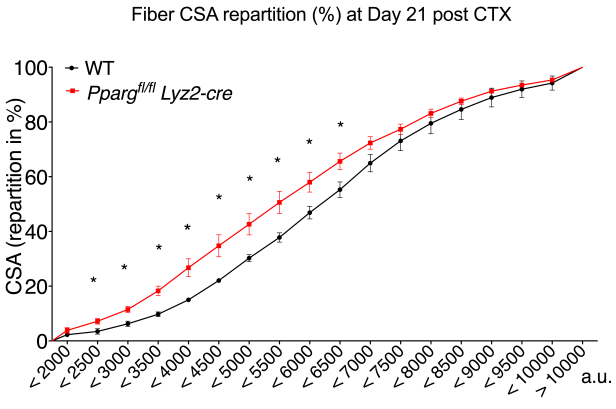
Fiber CSA repartition (%) at Day 21 post CTX
WT
Pparg fl/fl Lyz2-cre
CSA (repartition in %)
100
80
60
40
20
0
<2000
<2500
<3000
<3500
<4000
<4500
<5000
<5500
<6000
<6500
<7000
<7500
<8000
<8500
<9000
<9500
<10000
>10000
a.u.

B

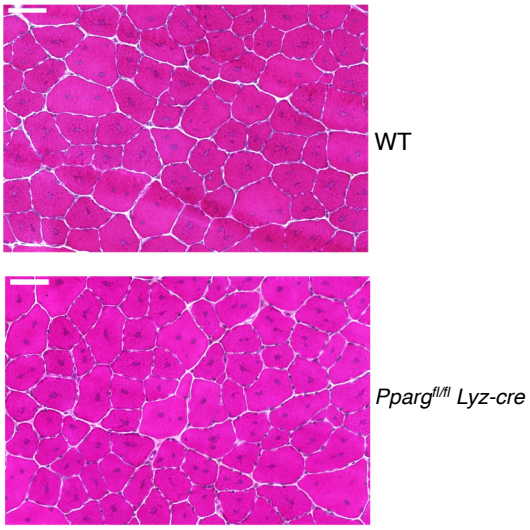
Day 21
WT
Pparg fl/fl Lyz-cre

C

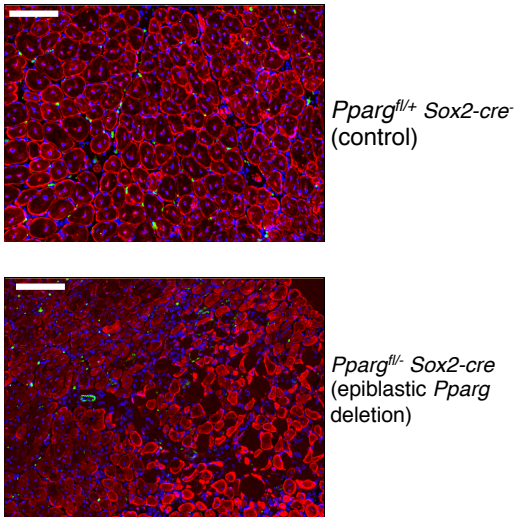
Day 8
Pparg fl/+ Sox2-cre-
(control)
Pparg fl/- Sox2-cre
(epiblastic Pparg
deletion)

Fig S2. related to Figure 1. Additional histological analysis of regeneration. Additional analysis to main Figure 1. (A) Cumulative CSA analysis of muscle section derived from WT or *Pparg*$^{fl/fl}$ *Lyz2-cre* animals at day 8 or day 21 post CTX injury. **(B)** Representative images of HE stained skeletal muscle from WT and *Pparg*$^{fl/fl}$ *Lyz2-cre* animals or post CTX induced injury (day 21) are shown. Scale bars represent 50 μm. n=5 and 6 for the day 8 *Pparg*$^{fl/fl}$ *Lyz2-cre vs.* WT comparison and 5 and 5 for the day 21 comparison. **(C)** IHC of desmin (red), F4/80 (green) and DAPI (blue) on muscle sections from full body *Pparg*$^{fl/+}$ *Sox2-cre*$^{-}$ (controls) and *Pparg*$^{fl/-}$ *Sox2-cre*$^{+}$ animals isolated at day 8 post CTX. Scale bars represent 100 μm.

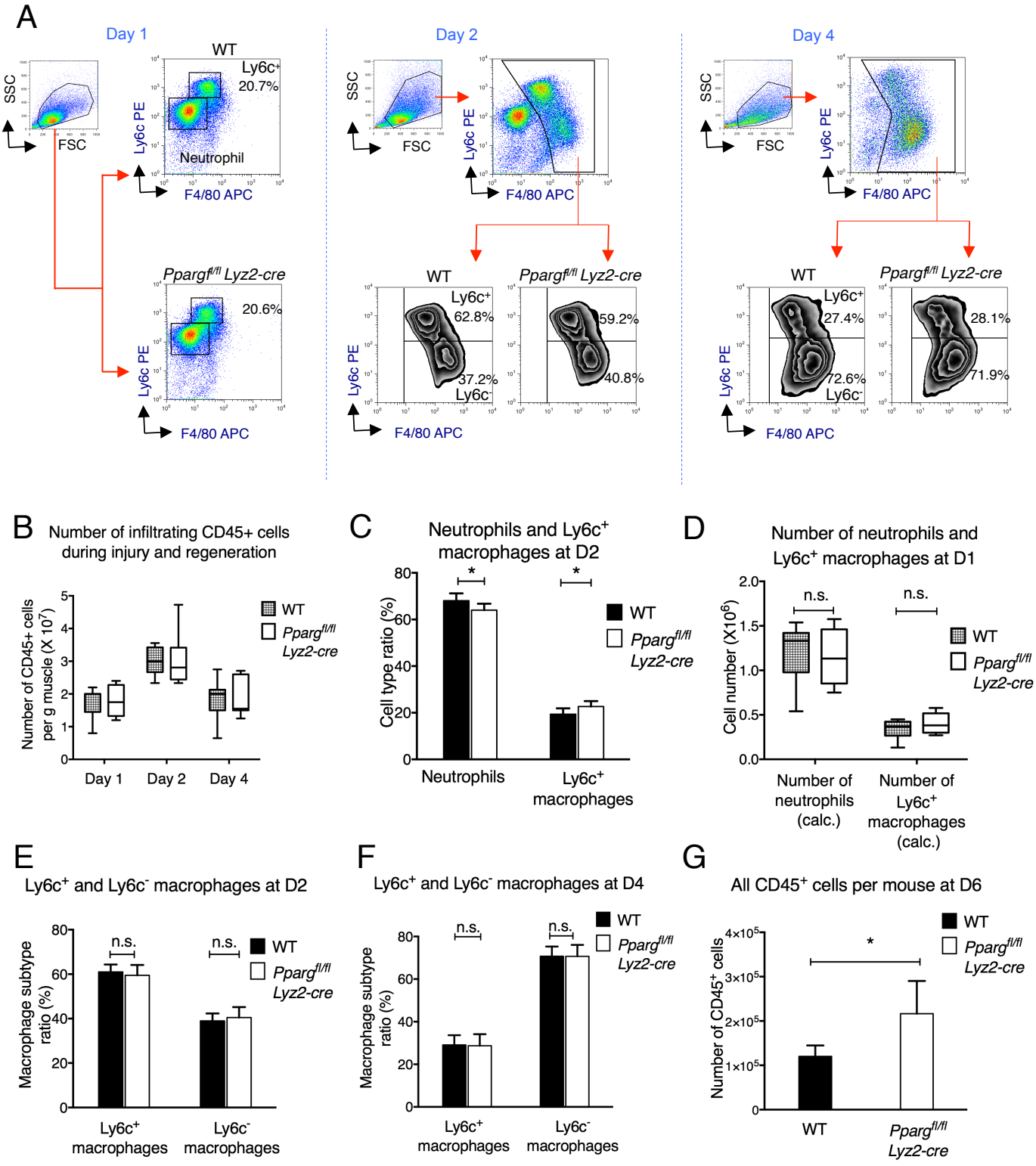

VARGA et al. Suppl Fig 3.

Fig S3. related to Figure 1. Analysis of macrophage infiltration and dynamics during regeneration (A) FACS gating strategy to enumerate muscle infiltrative neutrophils, and Ly6c^{+} and Ly6c^{-} macrophages at day 1, 2 and 4 post CTX. Representative samples and gate frequencies are shown. (B) Total number of infiltrating CD45^{+} hematopoietic cells isolated from CTX injured muscles of WT and *Pparg*$^{fl/fl}$ *Lyz2-cre* animals at day 1, day 2 and day 4. (D=day) n=8, 12 and 11 for WT animals and 8, 8 and 7 for *Pparg*$^{fl/fl}$ *Lyz2-cre* mice from days 1, 2 or 4. (C) Percentage of neutrophils and Ly6c^{+} macrophages and the (D) calculated neutrophil and macrophage numbers at day 1 in injured muscles. n= 8 for both genotypes. (E and F) Percentage of Ly6c^{+} and Ly6c^{-} macrophages in injured muscles at day 2 and day 4. n=8 for WT and 11 for *Pparg*$^{fl/fl}$ *Lyz2-cre* samples at day 2 and n=12 and 7 for WT and *Pparg*$^{fl/fl}$ *Lyz2-cre* mice at day 4. (G) number of CD45^{+} cells isolated from regenerating muscles at day 6. Bar graphs show mean values +/- SD. n=4 for both genotypes.

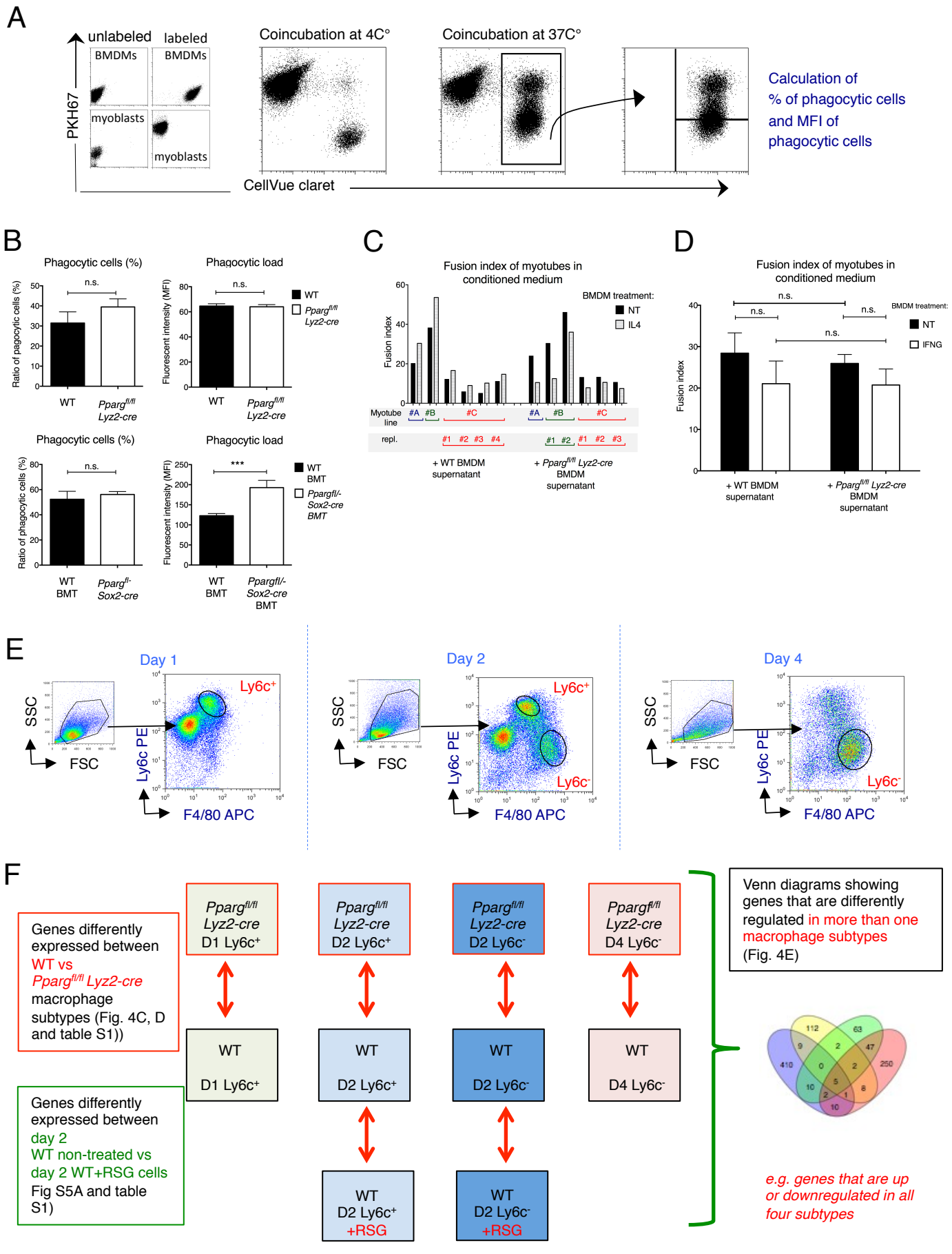

VARGA et al. Suppl Fig 4.

Fig S4. related to Figure 2. Analysis of macrophage derived effects on muscle regeneration (A) Experimental strategy to measure *in vitro* phagocytosis in BMDMs. (B) Percentage of phagocytic BMDMs and the Median Fluorescent Intensity (MFI) in the phagocytic BMDM compartment in BMDMs derived from WT *vs.* *Pparg*$^{fl/fl}$ *Lyz2-cre* (upper panel) or WT BMT vs *Pparg*$^{fl/+}$ *Sox-cre* BMT animals (Bottom panel). n=4 for each condition or genotype. FigS4 C, D, E and F provide additional information to main Fig. 2. (C) The pro-differentiation effect of IL4-treated BMDM supernatants on myoblast fusion is independent of the myoblast clone. The experiment was carried out on 3 independently isolated myoblast lines. (D) BMDM PPARγ does not modulate the effect of IFN-γ -treated BMDM supernatants on myoblast fusion. n=3 (E) FACS gating strategy for the sorting of macrophage subsets from CTX injured muscles (F) Schematics of the transcriptomic analyses of sorted muscle derived macrophage populations.

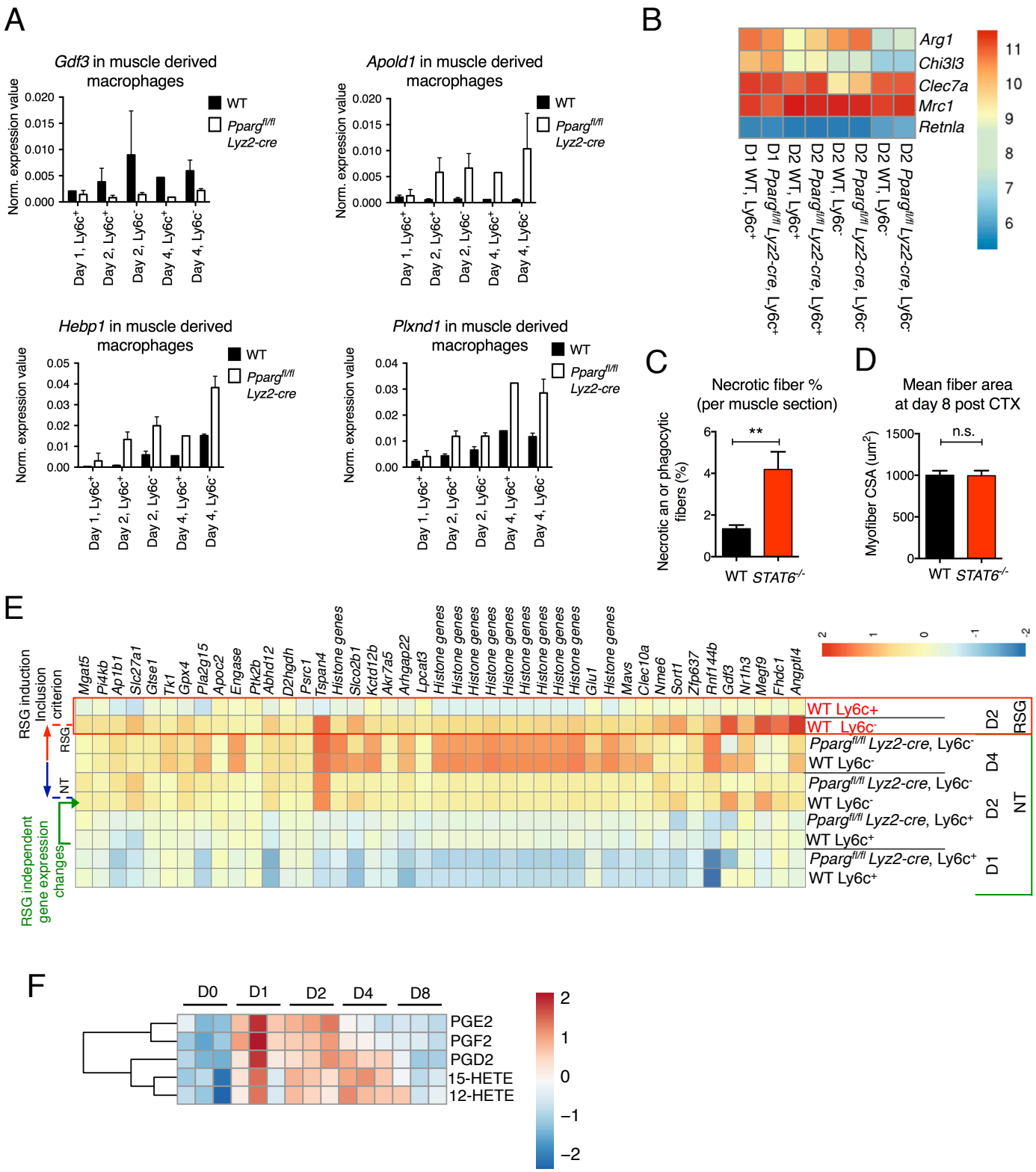
A
Gdf3 in muscle derived macrophages
Apold1 in muscle derived macrophages
Hebp1 in muscle derived macrophages
Plxnd1 in muscle derived macrophages
Norm. expression value
WT
Pparg fl/fl Lyz2-cre
Day 1, Ly6c+
Day 2, Ly6c+
Day 2, Ly6c-
Day 4, Ly6c+
Day 4, Ly6c-
B
Arg1
Chi3l3
Clec7a
Mrc1
Retnla
D1 WT, Ly6c+
D1 Pparg fl/fl Lyz2-cre, Ly6c+
D2 WT, Ly6c+
D2 Pparg fl/fl Lyz2-cre, Ly6c+
D2 WT, Ly6c-
D2 Pparg fl/fl Lyz2-cre, Ly6c-
C
Necrotic fiber %
(per muscle section)
Necrotic an or phagocytic fibers (%)
**
WT
STAT6-/-
D
Mean fiber area
at day 8 post CTX
Myofiber CSA (um2)
n.s.
E
RSG induction
Inclusion criterion
RSG
NT
RSG independent gene expression changes
Mgat5
Pi4kb
Ap1b1
Slc27a1
Gtse1
Tk1
Gpx4
Pla2g15
Apoc2
Engase
Ptk2b
Abhd12
D2hgdh
Psrc1
Tspan4
Histone genes
Slco2b1
Kctd12b
Akr7a5
Arhgap22
Lpcat3
Glu1
Mavs
Clec10a
Nme6
Sort1
Zfp637
Rnf144b
Gdf3
Nr1h3
Megf9
Fhdc1
Angptl4
WT Ly6c+
WT Ly6c-
Pparg fl/fl Lyz2-cre, Ly6c-
WT Ly6c-
Pparg fl/fl Lyz2-cre, Ly6c-
WT Ly6c-
Pparg fl/fl Lyz2-cre, Ly6c+
WT Ly6c+
Pparg fl/fl Lyz2-cre, Ly6c+
WT Ly6c+
D2
D4
D2
D1
RSG
NT
F
D0
D1
D2
D4
D8
PGE2
PGF2
PGD2
15-HETE
12-HETE

Fig S5. related to Figure 2. Additional analysis of the gene expression changes in sorted macrophage populations (A) RT-qPCR validation of the expression pattern of PPARγ-dependent genes in muscle derived sterile inflammatory macrophages. n=2, 8, 10, 1 and 4 (for day 1 Ly6c^{+}, day 2 Ly6c^{+}, day 2 Ly6c^{-}, day 4 Ly6c^{+} (pooled) and day 4 Ly6c^{-} cells) from WT and n= 5, 6, 7, 1 and 4 from *Pparg*$^{fl/fl}$ *Lyz2-cre* mice. (B) Expression of alternative macrophage markers in isolated macrophage subsets (C) STAT6 deficiency increases the number of necrotic/phagocytic fibers after CTX injury. (D) STAT6 deficiency does not impair CSA restoration after CTX injury. n= 6 or 7 for WT or *Stat6*$^{-/-}$ muscles. (E) Heatmap representation of the expression pattern of the genes that are upregulated by RSG treatment in WT Ly6c^{-} cells at day 2. Expression pattern of these genes are shown in all isolated macrophage subtypes. The RSG dependent induction is labeled with red/blue arrows on the left side. The induction in WT untreated day 2 Ly6c^{+} vs. Ly6c^{-} macrophages, which is reminiscent to the induction caused by RSG treatment, is labeled with a green arrow on the left side. Different *Hist2h3* isoforms are labeled as *Histone genes*. (F) Heatmap representation of lipid contents isolated from injured and regenerating muscles.

A

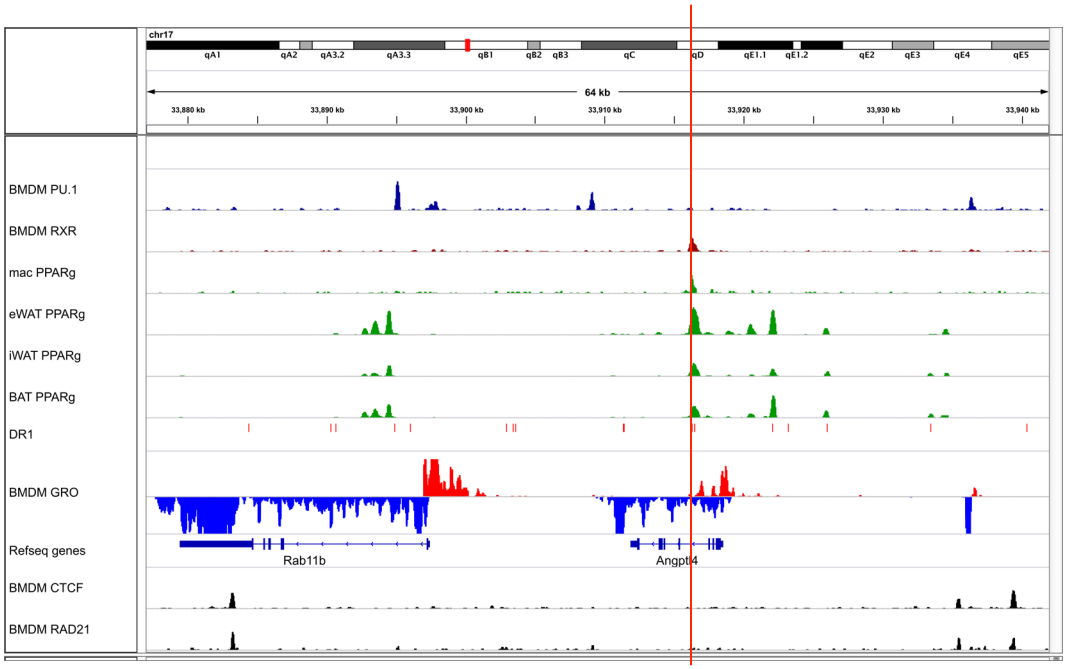

B

Distance from T.S.S. of *Gdf3*	BMDM PU.1 ChIPseq	BMDM RXR ChIPseq	Macrophage PPARG ChIPseq	Adipocyte PPARG ChIPseq (eWAT/iWAT / BAT)	DR1	BMDM H3K4me3	BMDM CTCF/RAD21
+38 Kb	+	+	-	+	-	+/-	-
+34 Kb	+/-	-	-	-	-	-	-
+16 Kb	+	-	-	-	-	-	-
+11 Kb	+	+	-	-	+	+	-
+10 Kb	+	+/-	-	+/-	-	+	-
+7.3 Kb	-	+/-	-	+/-	+	+	-
+5.4 Kb	+	+/-	-	-	-	+	
Gdf3							
-4.1 Kb	-	-	-	-	-	-	+
-21 Kb	+/-	+/-	+/-	+/-	+		
-25 Kb	+/-	+	+	+	-	-	-
-28 Kb	+/-	+	-	-	-	-	+/-
-40 Kb	+/-	+/-	-	-	-	-	-
-44 Kb	+	+	+/-	-	-	-	-
-47 Kb	+	+	+/-	-	-	-	-

VARGA et al. Suppl Fig 6.

Fig S6. related to Figure 3. Epigenomic analysis of enhancers regulated by PPARγ. Additional supportive information to main Fig. 3. **(A)** Identification of the active, PPARγ -regulated enhancer around the *Angptl4* locus. Red vertical line labels the relevant enhancer. **(B)** Enhancer selection scheme for identifying active enhancers around the *Gdf3* locus.

A

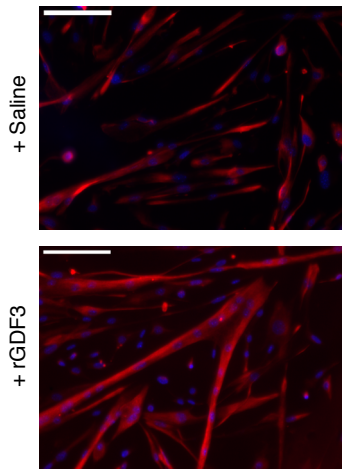

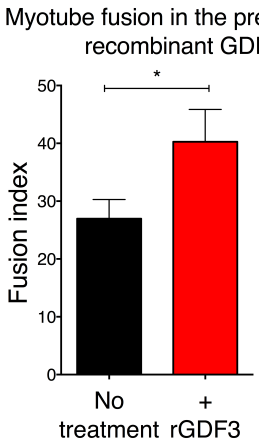

B

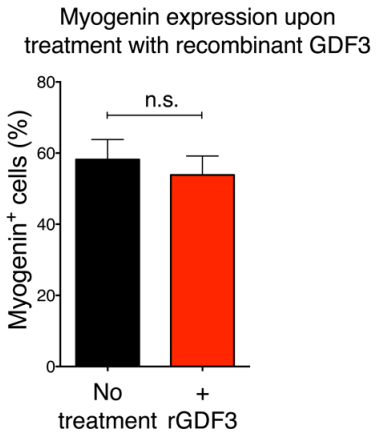

C

LIGANDS		LIGANDS	
Gdf1	growth differentiation factor 1	*Inhbc*	inhibin beta-C
Gdf2	growth differentiation factor 2	*Inhbe*	inhibin beta E
Gdf5	growth differentiation factor 5	*Amh*	anti-Mullerian hormone
Gdf6	growth differentiation factor 6	*Nodal*	nodal
Gdf7	growth differentiation factor 7		
Mstn	myostatin	RECEPTORS	
Gdf9	growth differentiation factor 9		
Gdf10	growth differentiation factor 10	*Acvr1c*	activin A receptor, type IC
Gdf11	growth differentiation factor 11	*Acvr2b*	activin receptor IIB
Tgfb2	transforming growth factor, beta 2	*Bmpr1a*	bone morphogenetic protein receptor, type 1A
Tgfb3	transforming growth factor, beta 3	*Bmpr1b*	bone morphogenetic protein receptor, type 1B
Bmp2	bone morphogenetic protein 2	*Amhr2*	anti-Mullerian hormone type 2 receptor
Bmp3	bone morphogenetic protein 3	*Tgfbr3*	transforming growth factor, beta receptor III
Bmp4	bone morphogenetic protein 4	*Tdgf1*	teratocarcinoma-derived growth factor 1
Bmp5	bone morphogenetic protein 5	*Hfe2*	hemochromatosis type 2
Bmp6	bone morphogenetic protein 6		
Bmp7	bone morphogenetic protein 7	ANTAGONISTS	
Bmp8a	bone morphogenetic protein 8a		
Bmp8b	bone morphogenetic protein 8b	*Chrd*	chordin
Bmp10	bone morphogenetic protein 10	*Lefty1*	left right determination factor 1
Bmp15	bone morphogenetic protein 15	*Lefty2*	left right determination factor 2
Inha	inhibin, alpha	*Nog*	noggin
Inhbb	inhibin beta-B	*Sost*	sclerostin

Fig S7. related to Figures 6 and 7. GDF3 and muscle regeneration. Fig. S7A and B provides additional analysis to main Fig. 6 C and D. **(A)** Effect of GDF3 on the fusion of primary myoblasts in an *in vitro* myoblast assay optimized for measurement of the myoblasts fusion step. Representative images (left panel) and fusion indexes (+/- SEM) (right panel) are shown. n=3. **(B)** Lack of induction in myogenin protein expression detected by IHC in differentiating myoblasts in the presence of GDF3 (Mean values +/- SEM). n=3. Fig. S7C provides additional data to main Fig. 7F. **(C)** List of members of the TGF-β superfamily signaling system that are not expressed in muscle derived macrophages.

SUPPLEMENTAL TABLE LEGENDS

Table S1. related to Figure 2. Gene expression analysis of muscle infiltrative macrophages isolated from regenerating muscles of WT and *Pparg*$^{fl/fl}$ *Lyz2-cre* animals. Both RAW data and "per gene normalized (*i.e*. normalized to the median expression value of respective gene") data are shown, after preliminary data processing of microarray data. Worksheet "Day 1 to 4 WT *vs*. PPARγ KO DATA" contains all data derived from macrophages isolated 1, 2 or 4 days post CTX treatment. Worksheet "Day 2 WT NT vs RSG DATA" contains all data derived from day 2 post CTX mice that were treated +/- RSG. "COMP" worksheets contain the list of genes that are differently expressed when the two respective 2 macrophage populations are compared (based on a 2 way ANOVA carried out on the whole data set). Genes with $p \leq 0.05$ were considered significant and are listed in the comparison worksheets.

Table S2. Related to Figure 7. Gene expression analysis of differentiating primary myoblast by RNA-Seq. Expression data from undifferentiated primary myoblasts, myoblasts differentiated for 1 day and myoblasts differentiated for 1 day in the presence of GDF3 were compared. Worksheet "MyB_all_expressed_genes_anova" lists expression values, p values and log2 fold change values for all genes that are differently expressed between any two conditions by 2 way ANOVA ($p \leq 0.05$). Worksheets "Mblast vs D1" and "D1 *vs*. D1 GDF3" contain the list of genes that are differently expressed between the two relevant conditions.

SUPPLEMENTAL MATERIALS AND METHODS

Mice. Genetically modified mice and wild type (WT) C57BL/6 controls were bred under SPF conditions and used for experiments in accordance with Hungarian (license no.: 21/2011/DE MÁB) and European regulations. Experiments were conducted on 2-4 month old male mice. Breeding of genetically modified *Gdf3*$^{-/-}$ and their control C57BL/6 albino animals, and the experiments with them were accepted and conducted with the permission of Sanford Burnham Prebys Medical Discovery Institute at Lake Nona IACUC approval (protocol No. 2014-0107).

Pparg$^{fl/fl}$*Lyz2-cre* and wild type C57BL/6 mice were used in most experiments. They were generated in *Pparg*$^{fl/fl}$*Lyz2-cre* X *Pparg*$^{fl/fl}$*Lyz2-cre* and WT X WT crossings. In a separate experiment, a small cohort of *Pparg*$^{fl/fl}$*Lyz2-cre* and littermate control *Pparg*$^{+/+}$*Lyz2-cre* animals were generated from *Pparg*$^{fl/fl}$*Lyz2-cre* X *Pparg*$^{fl/+}$*Lyz2-cre* crossings. The animals from this latter cohort were CTX injected and HE stained slides generated 8 days post CTX injections were visually evaluated in a double blind fashion. This experiment detected a delay in *Pparg*$^{fl/fl}$*Lyz2-cre* animals (*vs.* WT) that was indistinguishable from the delay seen in the *Pparg*$^{fl/fl}$*Lyz2-cre* samples generated in the non-littermate crossings.

Pparg$^{fl/-}$*Sox2-cre*$^{+}$ and littermate control *Pparg*$^{fl/+}$*Lyz2-cre*$^{-}$ animals were generated in (male) *Pparg*$^{+/-}$*Sox2-Cre*$^{+}$ X (female) *Pparg*$^{fl/fl}$*Sox2-Cre*$^{-}$ crossings.

Gdf3$^{-/-}$ and littermate C57BL/6 albino controls were generated in *Gdf3*$^{+/-}$ X *Gdf3*$^{+/-}$ crossings.

Stat6$^{-/-}$ animals and littermate C57BL/6 controls were generated in *Stat6*$^{-/-}$ X *Stat6*$^{-/-}$ *and* C57BL/6 X C57BL/6 crossings, respectively.

Muscle injury. Mice were anaesthetized with isoflurane and 50 µl of cardiotoxin (12X10^{-6} mol/l in PBS) (from Latoxan) was injected in the *tibialis anterior* (TA) muscle. Muscles were recovered for flow cytometry analysis at day 1, 2 or 4 post-injury or for muscle histology at day 8 post-injury. Glycerol injury was performed according to (Heredia et al., 2013); freeze injury was performed as described in (Hardy et al., 2016); crush injury was performed as in (Mitchell et al., 1992). In some experiments, 300 ng recombinant (r) GDF3 in 50 ul PBS, was injected at day 4 post-CTX into each TA muscle.

Histological analysis of muscle regeneration. Muscles were removed and snap frozen in nitrogen-chilled isopentane (–160°C). 8 µm thick cryosections were cut and stained with hematoxylin-eosin (HE).

Picture capture and counting. For each histological analysis, at least 5 slides (per condition) were selected where the total regernerative region within the CTX injured TA muscle was at least 70%. For each TA, myofibers in at least 3 fields randomly chosen in the entire injured area were counted and measured. HE muscle sections for the day 0, day 8 and day 21 *Pparg*$^{fl/fl}$*Lyz2-cre* vs. WT comparisons were recorded with a Nikon E800 microscope at 20X magnification connected to a QIMAGING camera. Cross-sectional area (CSA) measurement of these samples was carried out using Metamorph software and the CSAs are reported in arbitrary units. HE muscle sections for the day 16 and 20 *Gdf3*$^{-/-}$ BMT *vs*. WT BMT and for the day 22 *Pparg*$^{fl/-}$*Sox2-cre* BMT *vs.* WT BMT samples, the day 8 *Stat6*$^{-/-}$ and the *Pparg*$^{fl/fl}$*Lyz2-cre* + recombinant GDF3 injected

samples, were scanned with Mirax digital slide scanner and the CSA was measured with Panoramic Viewer software. The CSAs for these latter samples are reported in µm. Quantitative analysis of necrotic and/or phagocytic *vs.* centrally nucleated myofibers was performed using the Image J software and was expressed as a percentage of the total number of myofibers. Necrotic myofibers were defined as pink pale patchy fibers and phagocyted myofibers were defined as pink pale fibers, which are invaded by basophil single cells (macrophages).

Immunofluorescent detection of muscle regeneration in day 8 CTX injected muscle: Tissue sections were fixed and permeabilized in ice cold acetone for 5 min and blocked for 30 minutes at 20 °C (room temperature) in PBS containing 2 % bovine serum albumin (BSA). Tissues were stained for 1 h at room temperature using a primary antibody diluted in 2 % BSA. The primary antibodies used for immunofluorescence are listed in Supplementary Table 1. In all cases, the primary antibody was detected using secondary antibodies conjugated to FITC (JIR 712-095-153) or Cy3 JIR (711-165-152). The nuclei were counter stained with 0.1-1 µg/ml Hoechst. Fluorescent microscopy was performed using Carl Zeiss Axio Imager Z2 microscope equipped with lasers at 488, 568 and 633 nm. Figures were analyzed and assembled using Fiji and Illustrator CS5 (Adobe).

List of primary antibodies used in immunofluorescence:

Antibody	**Dilution**	**Source**
Rabbit anti-Desmin	1/200	Abcam (ab32362)
Rat anti-F4/80	1/400	Abcam (ab664)

Macrophage cell culture for conditioned medium generation. Macrophages were obtained from bone marrow (BM) precursor cells. Briefly, total BM was obtained from mice by flushing femurs and tibiae bone marrow with DMEM. Cells were cultured in DMEM medium containing 20% FBS and 30% conditioned medium of L929 cell line (enriched in CSF-1) for 7 days. Macrophages were seeded (at 50000 cell/cm^2 for all experiments) and were activated with IFN-γ (50 ng/ml) and IL4 (10 ng/ml) to obtain M1 and M2 macrophages, respectively, in DMEM containing 10% FBS medium for 3 days. After washing steps, DMEM serum-free medium was added for 24 h, recovered and centrifugated to obtain macrophage-conditioned medium.

Myogenic precursor cell (MPC) culture. Murine MPCs were obtained from TA muscle and cultured using standard conditions in DMEM/ F12 (Gibco Life Technologies) containing 20% FBS and 2% Ultroser G (Pall Inc). Briefly, TA muscles of young mice were opened and cleared of nerves/blood vessels/fascia etc. Muscle preparations were lightly digested with collagenase and the resulting cells were plated then serially expanded. For proliferation studies, MPCs were seeded at 10000 cell/cm^2 on Matrigel (1/10) and incubated for 1 day with macrophage-conditioned medium + 2.5% FBS or with 2.5% FBS medium containing GDF3 mouse recombinant protein (300 ng/ml; R&D 958-G3-010). Cells were then incubated with anti-ki67 antibodies (15580 Abcam), which were subsequently visualized using cy3-conjugated secondary antibodies (Jackson Immunoresearch Inc). For differentiation studies, MPCs were seeded at 30000 cell/cm^2 on Matrigel (1/10) and incubated for 3 days with macrophage-conditioned medium containing 2% horse serum or with 2% horse serum medium containing GDF3 mouse recombinant protein (300 ng/ml; R&D). Cells were then incubated with anti-desmin

antibodies (32362 Abcam), in combination with a cy3-conjugated secondary antibody (Jackson Immunoresearch Inc).

In vitro effects of GDF3 on myogenesis: Myogenic cell differentiation (i.e. myoblast commitment into differentiated myocytes) was evaluated as described earlier (Saclier et al., 2013). Cells were seeded at 30000 cells/cm2 in the presence of the absence of GDF3 (100 ng/ml) for 24h. Myogenin immunostaining (sc-12732, 1/20) was performed and the number of myogenin-positive nuclei was assessed for myogenic differentiation.

Myogenic cell fusion was evaluated as described earlier (Saclier et al., 2013). Cells were first seeded at 5000 cells/cm2 in differentiation medium and the differentiating myocytes were lifted and re-seeded at 75000 cells/cm2 in the presence of the absence of GDF3 (100 ng/ml) for 3 days. The number of nuclei in the myotubes was evaluated after desmin (AB32362 1/200) immunostaining and assessed for myogenic cell fusion.

P-SMAD2 signaling was evaluated in myogenic cell that have been cultured in the presence of the absence of GDF3 (100 ng/ml) for 6h. pSMAD2 (AB3849 Millipore,1/500) immunostaining was performed and the number of positive cells was counted.

Phagocytosis assay: BMDM cells were generated as described earlier in this section. BMDMs were harvested with trypsin and careful scraping, washed twice in PBS and then stained with the lipophilic fluorescent dye CellVue (Sigma) according to the manufacturer's recommendation. Stained BMDMs were replated and let to recuperate for one day in DMEM medium. C2C12 cells were cultured in DMEM containing 10% FBS. Cells were harvested, washed and stained with the lipophilic fluorescent dye PKH67

(Sigma). Stained C2C12 cells were washed extensively and then heat killed at 55°C for 60 min. Heat killed C2C12 cells were added to BMDM cultures at 2:1 ratio and phagocytosis was commence at 37°C or 4°C (controls). Cells were harvested by scraping after 1 h and fluorescent intensity was detected with a FACScalibur instrument.

Isolation of macrophages from muscle: Fascia of the TA was removed. Muscles were dissociated in RPMI containing 0.2% collagenase B (Roche Diagnostics GmbH) at 37°C for 1 hour and filtered through a 100 μm and a 40 μm filter. $CD45^+$ cells were isolated using magnetic sorting (Miltenyi Biotec). For cell sorting, macrophages were treated with Fcγ receptor blocking antibodies and with 10% normal rat serum: normal mouse serum 1:1 mix, then stained with a combination of PE-conjugated anti-Ly6c antibody (HK1.4, eBioscience) and APC-conjugated F4/80 antibody (BM8, eBioscience). $Ly6c^+$ $F4/80^{low}$ macrophages, $Ly6c^-$ $F4/80^+$ macrophages and $Ly6c^{mid}$ $F4/80^-$ neutrophils were sorted. In each experiment, both genotypes were processed in parallel to minimize experimental variation. Cells were analyzed and/or sorted with a BD FACSAria III sorter.

Isolation of macrophages and FAP cells from CTX injured muscles: CTX injured TA muscles were dissected and fat/nerves/fascias/tendons were discarded. Muscles were pulped and treated with a collagenase/dispase cocktail. $CD45^+F4/80^+$ macrophages and $CD45^-CD31^-Sca1^+PDGFRA(CD140)^+$ FAPs were sorted for RNA isolation.

RNA isolation from sorted MFs. MF subsets were sorted from day 1, 2 and 4 post-injury muscles with a FACSAria III sorter and total RNA was isolated with TRIZOL reagent according to the manufacturer's recommendation. 20 ug glycogen (Ambion) was added as a carrier for RNA precipitation.

Microarray analysis of muscle macrophages: Global expression pattern was analyzed on Affymetrix GeneChip Mouse Gene 1.0 ST arrays. Ambion WT Expression Kit (Life Technologies, Hungary) and GeneChip WT Terminal Labeling and Control Kit (Affymetrix) were used for amplifying and labeling 150 ng of total RNA. Samples (n=3, 4 or 5) were hybridized at 45 ºC for 16 h and then standard washing protocol was performed using Affymetrix GeneChip Fluidics Station 450. The arrays were scanned on GeneChip Scanner 7G (Affymetrix). Microarray data (data acess: GSE44057) were analyzed with GeneSpring 12 GX software (Agilent BioTechnologies). Affymetrix CEL files were normalized with Robust Multichip Analysis (RMA) algorithm and median normalization.

The microarray data are publicly available (Data access: GSE71155).

Expression data processing and analysis: Data quality control and analysis was carried out following the recommendations put forward in the Imgen website (http://www.immgen.org/Protocols/ImmGen%20QC%20Documentation_ALL-DataGeneration_0612.pdf).

Data were loaded into the Genespring GX software and RMA summarization was carried out. Next, a set of filtering steps was applied to the dataset. Briefly, data distribution curve was generated and the lowest 5% of the entities with detectable signals were filtered out as not expressed. Duplicate entities, not/poorly annotated transcripts and transcripts reporting inconsistent expression values were also discarded. Further analysis was carried out on the filtered dataset. Data was analyzed either based on the RAW expression values or after following a “per gene” normalization (individual gene expression data normalized to the median of the gene).

Further analysis of gene expression and comparisons were made either within Genespring GX or using the R software package. 2-way anova tests were performed in R using functions aov and TukeyHSD of package MASS, Heatmaps were drawn with package pheatmap. Statistically significant difference was considered if $p < 0.05$.

Microarray validation by RT-qPCR: Transcript quantification was performed by quantitative real-time RT (reverse transcriptase) PCR (polymerase chain reaction) using SYBR Green assays (*Apold1, Hebp1 and Plxnd1*) or PrimeTime assays from IDT (*Gdf3 and Pparg*). Primer sequences and Taqman probes or PrimeTime assay IDs used in transcript quantification are available upon request. RT-qPCR results were analyzed with the standard delta Ct method and results were normalized to the expression of *Actb*.

Identification and quantification of lipid mediators by liquid chromatography-tandem mass spectrometry. Tibialis anterior muscles collected after CTX-induced injury were minced in ice-cold methanol and stored at -80°C. Internal deuterium-labeled standards, including d_8-5-HETE and d_4-PGE_2, were then added to assess extraction recovery and quantification. Solid phase extraction and LC-MS/MS analysis were carried out essentially as described in (Colas et al., 2014). Briefly, lipid mediators were extracted by C18 column chromatography and methyl formate fractions were taken to dryness under a stream of N_2 gas prior to suspension in methanol:water (50:50). Samples were profiled using a high performance liquid chromatograph (HPLC, Shimadzu) coupled to a QTrap5500 mass spectrometer (AB Sciex). The instrument was operated in negative ionization mode and lipid mediators were identified and quantified using multiple reaction monitoring (MRM) transitions (Colas et al., 2014) after normalization to extraction recovery based on internal deuterium-labeled standards and

external calibration curves for each mediator. The specific MRM transitions used were: PGE_2 (351>175), PGD_2 (351>233), $PGF_{2\alpha}$ (351>193), 15-HETE (319>219) and 12-HETE (319>179).

Macrophage cell culture for ChIP: Macrophages were obtained from bone marrow (BM) precursor cells. Briefly, total BM was obtained from mice by flushing femurs and tibiae bone marrow with DMEM. Cells were RBC lysed with ACK solution and then plated on non-tissue culture grade plates then cultured in DMEM medium containing 20% FBS and 30% conditioned medium of L929 cell line (enriched in CSF1) for 6 days. Macrophages were harvested from the culture plates and ChIP was carried out.

ChIP (Chromatin immunoprecipitation): Cells were double crosslinked with 0,002M DSG (Sigma) for 30 minutes and then with 1% formaldehyde (Sigma) for 10 minutes. Nuclei were isolated with ChIP Lysis Buffer (1% Triton x-100, 0.1% SDS, 150 mM NaCl, 1mM EDTA, and 20 mM Tris, pH 8.0) then chromatin were sonicated (also in ChIP Lysis Buffer) with Diagenode Bioruptor to generate 200-1000 bp fragments. Chromatin was diluted in ChIP Lysis buffer and immunoprecipitated with antibodies against pre-immune IgG (Millipore, 12-370), (pan) RXR (sc-774 Santa Cruz Biotechnology) and PPAR gamma (Perseus #PP-A3409A). Chromatin antibody complexes were precipitated with Protein A coated paramagnetic beads (Life Technologies). Chromatin antibody complexes were washed on the beads once in IP Wash Buffer 1 (1% Triton, 0.1% SDS, 150 mM NaCl, 1 mM EDTA, 20 mM Tris, pH 8.0, and 0.1% NaDOC), twice in IP Wash Buffer 2 (1% Triton, 0.1% SDS, 500 mM NaCl, 1 mM EDTA, 20 mM Tris, pH 8.0, and 0.1% NaDOC) and once in IP Wash Buffer

3 (0.25 M LiCl, 0.5% NP-40, 1mM EDTA, 20 mM Tris, pH 8.0, 0.5% NaDOC) and IP Wash Buffer 4 (10 mM EDTA and 200 mM Tris, pH8.0). DNA fragments were then eluted and column purified (Qiagen, MinElute). DNA was applied for QPCR analysis. QPCR results were analyzed with the standard delta Ct method and results were normalized to input signals.

Bioinformatic analysis of the active enhancers around the *Gdf3* and *Angptl4* locus: Primary analysis of the raw sequence reads has been carried out using our ChIP-seq analysis command line pipeline. Alignment to the mm9 assembly of the mouse genome was done by the Burrows–Wheeler Alignment (BWA) tool. Genome coverage (bedgraph) files were generated by makeTagDirectory and makeUCSCfile.pl (HOMER) and were used for visualization with IGV2. Putative DR1 elements (reaching score 9) were determined by annotatePeaks.pl (HOMER) using the RXR and PPARg motif matrices of HOMER. The following datasets were used for the identification of active enhancers:

Sample name	SRA identifier	GEO identifier	Cell/tissue type	Sample type	Antibody
BMDM_PU.1	SRX651749	-	bone marrow derived macrophage	ChIP-seq	PU.1
BMDM_RXR	SRX651739	-	bone marrow derived macrophage	ChIP-seq	RXR
mac_PPARg	SRX019134	GSM532739	peritoneal macrophage	ChIP-seq	PPARg
eWAT_PPARg	SRX193440	GSM1018066	epididymal white adipose tissue	ChIP-seq	PPARg
iWAT_PPARg	SRX193441	GSM1018067	inguinal white adipose tissue	ChIP-seq	PPARg
BAT_PPARg	SRX193442	GSM1018068	brown adipose tissue	ChIP-seq	PPARg
BMDM_CTCF	SRX651751	-	bone marrow derived macrophage	ChIP-seq	CTCF
BMDM_RAD21	-	-	bone marrow derived macrophage	ChIP-seq	RAD21
BMDM_H3K4me3	SRX651747	-	bone marrow derived macrophage	ChIP-seq	H3K4me3
BMDM_GRO-seq	SRX651735	-	bone marrow derived macrophage	GRO-seq	-

Western Blotting: GDF3 protein expression was measured using Western Blot analysis. The Tibialis anterior (TA) was removed from mice injected intramuscularly with cardiotoxin (CTX) at experimental time points and homogenized in RIPA buffer. $CD45^{+/-}$ cell populations were isolated from whole TA muscle using MACS Micro Magnetic Bead Separation system (Bergisch Gladbach, Germany). Cell populations were collected and lysed in RIPA buffer. Protein concentrations were determined by Qubit 2.0 Fluorometer Protein Assay (Life Technologies, Carlsbad, CA). Protein samples were prepared for SDS-PAGE with 2X Laemmli Sample Buffer (Bio-Rad, Hercules, CA) at a 1 mg/ml concentration. SDS-PAGE was completed using 4-20% Mini Protean TGX gels (Bio-Rad, Hercules, CA) at 110 volts for 1 hour. The SDS-PAGE gel was then transferred onto PVDF membrane (Thermo Fisher, Waltham, MA) at 0.35 amps for 1-2 hours at 4°C. Membranes were blocked in 5% BSA in TBS-T at room temperature for >1 hour. GDF3 was targeted using rabbit monoclonal Anti-GDF3 primary antibody (ab109617, Abcam, Cambridge, MA) at 1:1,000 dilution in 5% BSA/TBS-T overnight at 4°C. Anti-GAPDH mouse monoclonal primary antibody (AM4300, Ambion, Carlsbad, CA) was used as a protein loading control at 1:10,000 – 1:20,000 dilution in 5% BSA+TBST overnight at 4°C. Membranes were washed 3X with TBS-T for 5 minutes each for a total of 15 minutes. Goat Anti-Rabbit HRP secondary antibody was used for the detection of GDF3 at 1:10,000 dilution in 5%BSA+TBS-T at room temperature for 1 hour. Anti-Mouse HRP secondary (Cell Signaling, 7076S) and Donkey Anti-Mouse Alexa Fluor 680 secondary (ab175774) antibodies were used for the detection of GAPDH at 1:40,000 dilution at room temperature for 1 hour. Membranes were washed 3X with

TBS-T for 5 minutes each for a total of 15 minutes, followed by 2 washes in TBS for 5 minutes. Super Signal West Pico Kit allowed for ECL visualization of the blot on Hyblot CL Film (Denville, E3018).

RNA sequencing (RNA-Seq) library preparation for myoblast gene expression analysis: Myoblast cells were plated at 30.000/cm2. After cell adhesion, medium was replace to differentiation medium (DMEM/F12 containing 2% horse serum). After overnight differentiation, 150 ng/ml GDF3 was added to selected wells. Cells were harvested in trizol in 24h and RNA was isolated following the suppliers's recommendations. cDNA library for RNA-Seq was generated from 1μg total RNA using TruSeq RNA Sample Preparation Kit (Illumina, San Diego, CA, USA) according to the manufacturer's protocol. Briefly, poly-A tailed RNAs were purified by oligodT conjugated magnetic beads and fragmented on 94 C degree for 8 minutes, then 1st strand cDNA was transcribed using random primers and SuperScript II reverse transcriptase (Lifetechnologies, Carlsbad, CA, USA). Following this step, second strand cDNA were synthesized and then double stranded cDNA molecules were end repaired resulting blunt ends. The 3' ends of the dscDNA molecules were adenylated then Illumina TruSeq index adapters were ligated. After adapter ligation step, enrichment PCR was performed to amplify the adapter-ligated cDNA fragments. Fragment size distribution and molarity of the libraries were checked on Agilent BioAnalyzer DNA1000 chip (Agilent Technologies, Santa Clara, CA, USA).

10 pM of denatured libraries were used for cluster generation on cBot instrument, then single read 50bp sequencing run was performed on Illumina HiScan SQ instrument (Illumina, San Diego, CA, USA).

The RNA-Seq data are publicly accessible (data access: PRJNA290560/SRR2136645).

RNA-seq bioinformatics analysis: The TopHat-Cufflinks toolkit was used for mapping spliced reads, making transcript assemblies, getting and sorting gene expression data. Genes with RPKM>=1 (at least in one sample) were considered to be expressed. 2-way ANOVA tests were performed in R using functions aov and TukeyHSD of package MASS, Heatmaps were drawn with package pheatmap.

General statistical analyses. All experiments were performed using at least three different samples. Student's t-tests and 2 way ANOVA analyses were performed and $P<0.05$ was considered significant ($P<0.05$=*, $P<0.01$=**, $P<0.001$=***). Mean and SD values, or mean and SEM values are shown in graphs.

Colas, R.A., Shinohara, M., Dalli, J., Chiang, N., and Serhan, C.N. (2014). Identification and signature profiles for pro-resolving and inflammatory lipid mediators in human tissue. American journal of physiology Cell physiology *307*, C39-54.
Hardy, D., Besnard, A., Latil, M., Jouvion, G., Briand, D., Thepenier, C., Pascal, Q., Guguin, A., Gayraud-Morel, B., Cavaillon, J.M*., et al.* (2016). Comparative Study of Injury Models for Studying Muscle Regeneration in Mice. PloS one *11*, e0147198.
Heredia, J.E., Mukundan, L., Chen, F.M., Mueller, A.A., Deo, R.C., Locksley, R.M., Rando, T.A., and Chawla, A. (2013). Type 2 innate signals stimulate fibro/adipogenic progenitors to facilitate muscle regeneration. Cell *153*, 376-388.
Mitchell, C.A., McGeachie, J.K., and Grounds, M.D. (1992). Cellular differences in the regeneration of murine skeletal muscle: a quantitative histological study in SJL/J and BALB/c mice. Cell and tissue research *269*, 159-166.

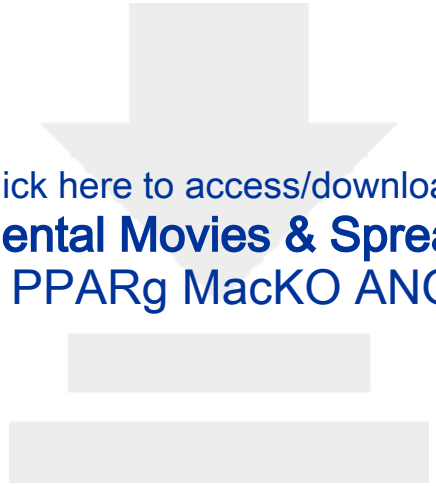

Click here to access/download

Supplemental Movies & Spreadsheets

Table S1 PPARg MacKO ANOVA .xlsx

Supplemental Spreadsheets

Click here to access/download

Supplemental Movies & Spreadsheets

Table S2 Myoblast diff ANOVA.xlsx